EUROPEAN COMMISSION
5th EURATOM FRAMEWORK PROGRAMME 1998-2002
KEY ACTION : NUCLEAR FISSION

HTR-M

European Project for the development of HTR Technology - Materials for the HTR

CONTRACT N°
FIKI-CT-2000-00032
&
FIKI-CT-2001-00135

Results of testing and irradiation behaviour of Mod 9Cr 1 Mo steel RPV welds and base material

By

J. B.J.W. Hegeman (NRG)
H. Rantala (JRC)
Netherlands

Dissemination level : CO
Document Number: HTR-M-04/10-D-1.4.99
Deliverable 1.5

Modified 9Cr steel for HTR

Reference testing and irradiation behaviour

J.B.J. Hegeman
J.H. Rantala
F.P. van den Broek
J. Boskeljon
P. ten Pierick
R. den Boef

Petten, 7 September 2004

20585/05.64311/P

Under the Nuclear Energy RTD programme of the EC, contract N° FIKI-CT-2000-00032, deliverable 1.5: Complementary irradiation data on the properties of one HTR base material and weld

author :	J.B.J. Hegeman	reviewed :	J.W. Rensman
66 page(s)	MMI/HHe/NO	approved :	B. van der Schaaf
modified 9cr steel for htr (2).doc			

© NRG 2004

Subject to agreement with the client, the information contained in this report may not be disclosed to any third party and NRG is not liable for any damage arising out of the use of such information.

Contents

List of tables

List of figures

Summary

In the frame of the HTR-m programme a thick welded joint of modified 9Cr was produced by Framatome ANP. Modified 9Cr is a candidate Reactor Pressure Vessel steel for the hot vessel option of a High Temperature Reactor (HTR). In the programme, the main objective was to study the irradiation behaviour of the weldment because the weldment is identified as the weakest zone of the pressure vessel.

HTR representative irradiation and testing conditions have been chosen, such as room temperature tests, 375°C (minimum vessel operating temperature), 450°C (maximum vessel operating temperature) and 550°C for of-normal conditions. The mechanical tests comprised tensile, creep, impact and fracture toughness tests of various orientations and material conditions. The irradiation took place in the Pool Side Facility of the High Flux Reactor, Petten, at 375°C up to a fluence of $9.44 \cdot 10^{22}$ m^{-2} (E>0.1MeV), i.e. the end of life condition of the HTR-reactor pressure vessel.

This report elaborates on the results from the reference tests (by JRC.IE) and on the results for the mechanical testing on irradiated specimens (by NRG/MMI). Moreover, the irradiation history and rig loading is reported. Tensile tests at room temperature showed an increase of yield strength due to irradiation of 40 MPa, while at higher temperatures negligible hardening was observed. The irradiation effect on creep properties at 550°C is small, i.e. within the scatter band. An increase of upper shelf energy was observed from impact tests. The irradiation resulted in an insignificant shift of transition temperature of about +10°C. High fracture toughness was observed from CT fracture toughness testing. Compared with reference results of commercial 9Cr. steel, obtained within the frame of other research programmes, the effect of neutron irradiation is expected to be small.

This report covers deliverable 1.5: Complementary irradiation data on the properties of one HTR base material and weld.

This research has been carried out under contract N° FIKI-CT-2000-00032 under the Nuclear Energy RTD programme of the EC, with additional financial support from the Ministry of Economic Affairs of the Netherlands.

1 Introduction

The development of Advanced High Temperature Reactor (HTR) concepts requires material data and an understanding of the material behaviour under reactor operating conditions and environment. For components important to the safety and feasibility of designs, such as the main steel structures (vessel, internal structures, turbine) and the graphite structures (core), investigation of the behaviour of the different materials in the reactor environment is a necessary requirement. This work identifies and investigates the candidate materials and provides an HTR database of properties for the materials of the key components that can be used by designers for feasibility investigations of the most promising options for future application. This part of the project mainly focuses on the Reactor Pressure Vessel (RPV) for the HTR.

The reactor pressure vessel in the high temperature reactor will be irradiated with neutrons, which cause damage within the material and will result in a change in mechanical behaviour of these materials. Depending on the operating conditions of the HTR, this irradiation takes place at temperatures between 120°C and 450°C, where 120°C is the lower temperature of the "cold-vessel" option, 375°C the lower temperature for the 'hot-vessel' option and 450°C the upper end of the temperature operating window of the hot-vessel. In accidental conditions the temperature of the vessel might increase up to 600°C. At the lower temperatures, the embrittlement and integrity of the RPV-material and welded joints should be studied. At the higher temperature the creep behaviour of the RPV material and the weldments is an important factor in determining the lifetime of the HTR and the vessel behaviour under abnormal conditions. The objective is therefore to confirm the choice of material for different HTR concepts (in the present investigation, mod. 9Cr 1Mo for the 'hot-vessel' option), in relation to both normal and accident conditions, and compile their design properties.

The main objective of the project is to improve the reactor pressure vessel of the HTR by design, structural integrity analysis and provide the materials properties currently lacking. Additionally, the objective is to develop HTR vessel materials and data in the areas of design analysis, structural integrity analysis and materials properties under HTR conditions including testing on welds for cold and hot vessel options.

In this report the experimental data acquired in the HTR-m programme is presented. The lowest temperature of the vessel-operating window is chosen for irradiation because it is expected that the mod.9Cr steel is most susceptible to irradiation embrittlement at these temperatures. The test matrix has been optimised for the HTR "hot vessel" option. The irradiation and test-matrix is tailored to deliver complementary data to the RCC-MR and ASME design code. In various reports, the missing data has been identified and analysed in the frame of the HTR project [1][2][7][8] in addition to studies on the HTR environment, damage mechanisms and sensitive zones [3]-[6]. It was concluded that mainly the irradiation behaviour of the welded joints should be addressed. The results of the reference tests and irradiation tests are given in this report.

2 Experimental set-up and test matrix

Specimens for mechanical testing were selected from a weldedjoint produced by Framatome ANP [14]. The weldment was produced by narrow cap TIG welding on modified 9% Chromium steel (P91). The postweld heat treatment is 10h30 at 760°C following the report in reference [14]. The plate is 150 mm thick and the weldment has a length of approximately 1 m. In order to study the mechanical behaviour of such a weldment the following assessment was made: The heat affected zone (HAZ) and the weld metal are identified as critical zones, i.e. those regions are most susceptible to crack initiation and growth. The test matrix, types of specimens are reported in [11]. The Material specification is given in appendix A.

2.1 Final specimen selection and cutting scheme

Four material conditions have been selected for the mechanical testing: plate material, in parallel and in perpendicular direction with respect to the rolling direction, the heat affected zone (HAZ) and the weld metal. For each specimen type a detailed description on the orientation and the test conditions is given in [11]. The specimen geometry for reference testing and for post irradiation examination have been the same for all the specimen types to enhance the comparison between the EOL condition and reference condition.

The material conditions selected for testing are: tensile and creep specimens in two plate directions L and T, full-weld metal and cross the weld specimens. The notched specimens (CT fracture toughness and (sub-size) charpy were cut with the notch in the base metal (plate) in the L-T and T-L orientation, with the notch in the HAZ and full weld metal in the welding direction.

The test matrix is summarised in table 1 and the detailed cutting schemes for specimen retrieval are shown in figure 41 to figure 48 in appendix F. The identification number of the specimen is related to its location within the welded joint and plate. The total number of specimens was limited (budget) and additional mechanical tests are required (6^{th} FP) for the qualification of P91 and the welded joint as a candidate pressure vessel steel for the HTR.

After welding a few hot-cracks were observed from metallographic examinations of cut surfaces [14][17]. Therefore it was decided to inspect the plates for defects using non-destructive techniques to avoid machining of specimens that have to be excluded during the testing phase. The thick welded plate was cut in thinner plates, figure 41, and then ultrasonically inspected for crack/defects. The excluded zones are indicated in the cutting schemes.

Due to a misalignment during the cutting of plate 2 into blocks, the specimens that were supposed to have the notch inside the HAZ, have the notch inside the weld metal, i.e. in the centre of the welded joint. Because of the limited amount of material available from the welded joint (the total welded joint had a length of ~1 m), HAZ notched sub-size specimens were cut from the full-size charpy specimens of plate 2, see figure 44. In this way, 40 KLST type (sub-size) specimens were produced with the notch located in the HAZ. Additionally, 4 full-size charpy specimens could be machined with the notch inside the HAZ. Only 11 full-size Charpy specimens were machined with the notch in the weld metal. In addition to the proposed test matrix, 4 CT specimens with a commercial grade 9Cr-1Mo steel (T91) have been added for comparison [13].

In the cutting schemes in appendix F, the blue marked specimens have been used for the irradiation, yellow for reference testing, green as dummy specimens to check testing equipment. The red marked specimens have been cut with the notch in the centre of the weld instead of in the HAZ. From these sub-size (KLST type) specimens have been produced from the misaligned full-size charpy specimens.

table 1 HTR-m test matrix for reference and irradiation testing

Specimen type	#	conditions	Temp.	**sub-total**	6^{th} FP	irr/ref	**total**
Small size Charpy (KLST)	15	4		**85**		irr & ref	**170*[1]**
Tensile	2	4	4	**32**		irr & ref	**64**
Creep	4	4	1	**16**	16*[2]	irr & ref	**32 (32*[2])**
Fracture toughness (CT10)	5	4	2	**20**		irr & ref	**40*[3]**
full-size Charpy	11	3		**25**	25	irr & ref	**50*[4]**

*1 15 Specimens in each plate direction L-T and T-L, 15 specimens in the weld metal, 40 specimens in the Heat Affected Zone (HAZ).

* 2 16 specimens have been irradiated but will be tested in the 6^{th} framework programme, also 16 additional creep specimens will be prepared for reference testing in the 6^{th} FP.

*3 four additional CT specimens of commercial T91 have been irradiated for comparison (see also a report on ADS window materials [13])

*4 25 additional full-size Charpy specimens have been included in the irradiation rig (for 6th FP bending or impact testing in Eastern Europe through JRC.IE) and 25 specimens for reference testing, hence 12 specimens of base material in T-L orientation, 11 specimens with the notch in the weld metal and 2 specimens with the notch in the HAZ for both irradiation and reference testing

2.2 Testing facilities and procedures

2.2.1 Tensile testing

For the tensile testing of the un-irradiated reference specimens at JRC a mechanical testing rig (ST-6), equipped with a 100kN-loadcell and a bulb-furnace was used to carry out the required tests. To install the specimen into the testing rig, special attachment pieces have been made. These attachment pieces were specially designed to avoid misalignment by using self-aligning spherical cup-cones.

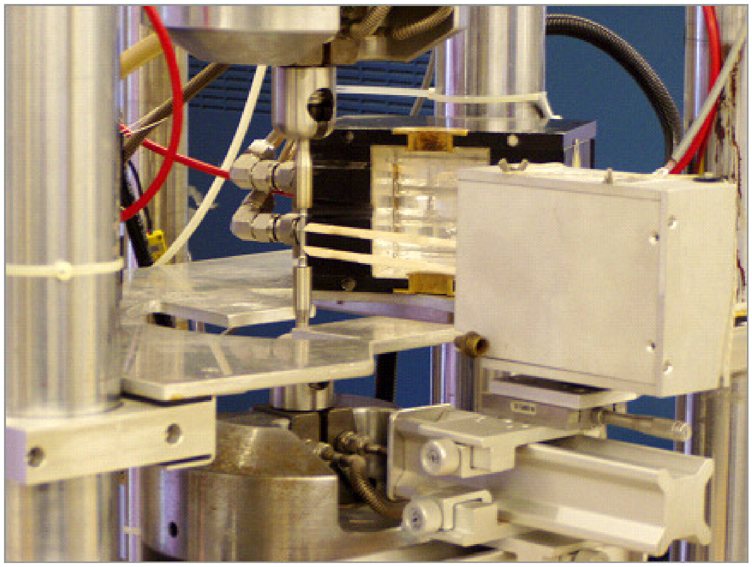

figure 1 The test set-up for the tensile testing of the un-irradiated reference specimens at JRC. Details of the flexible threaded grips, the extensometer and the bulb furnace are shown.

The tensile tests of the irradiated specimens were performed on an electromechanical test machine (Instron) equipped with a 10 kN load cell, located in the lead shielded hot cell of the NRG Hot Cell Laboratories. A split three-zone furnace mounted around the specimen was used to test the materials at elevated temperatures. The temperatures were controlled within ± 2 °C. The tests were performed in accordance with the ASTM standard for tension testing of metallic materials E8M. For reference testing, failure occurred at the contact point of the extensometer due to a contact pressure. This produced fracture strain readings, which are not completely representative. No extensometer has been used during testing of the irradiated specimens. It is normally assumed that during the test all plastic deformation takes place within the gauge length of the specimen. Therefore, the elongations (fracture and uniform) are related to the original size of the gauge length. The plastic strain after fracture was measured and compared with the recorded strains.

The 0.2% yield stress (0.2% YS), the ultimate tensile strength (UTS), and the fracture elongation (FE) are determined from the recorded stress-strain curves. The uniform (plastic) elongation (UE) is obtained from the plastic elongation at maximum load using the crosshead displacement. The reduction of area (RA), uniform reduction of area (URA) and the total elongation (TE) are measured from the broken test pieces. It should be mentioned that all reported strains are plastic strains.

After tensile testing, the smal identification numbers appeared to be unreadable due to irradiation and subsequently heating during testing. Therefore, the reduction of area and measured fracture elongation could not be determined for all of the specimens but only for those where the numbers were still readable. The various martensitic steels were tested at room temperature, 375°C - the irradiation temperature, 450°C - the estimated maximum vessel operating temperature; and 550°C - the creep temperature in accidental condition, see [11]. The initial strain rate was $5x10^{-4}$ s^{-1} where the machine crosshead displacement is constant.

2.2.2 Creep testing

For the reference creep testing at the JRC.IE laboratories the European Creep Collaborative Committee (ECCC) Recommendations have been used [20]. Dead weight loaded constant load creep machines have been used with an extensometer system fitted on the shoulders of the creep specimens. Ceramic extension arms transferred the movement outside (below) the furnace where two digital LVDT's have been used to measure the displacement. The effective gauge length is calculated according to the ECCC recommendations, Vol. 3, ch. 5.1. The specimens were heated to 550°C by three-zone resistance furnaces. Temperature was measured by two metal sheet thermocouples wound on the specimen. The temperature stability was better than +/- 1°C. The datalogging speed was set such that during the test 1000 data points would be saved. Alarm limits were also set in order to record all rapid deviations from the last saved results, which for example activated data saving at the end when strain rate accelerated rapidly towards the end. All equipment have been calibrated according to the quality system of the Institute. The temperature deviation measured during the calibration was compensated for. One material condition was tested in one machine only.
The procedure described by R. Bestwick [16] has been used successfully to predict test stresses on the basis of the previous results.

The minimum strain rate is calculated manually in Excel by selecting a linear portion of the strain-time curve and then fitting a linear trendline through the selected data set. Failure strain was measured by carefully recombining the two specimen halves under a microscope and then measuring the elongation and the reduced diameter at the failure location using a digital x-y table of the microscope. The irradiated specimens have not been measured after fracture

The creep tests on the irradiated specimens have been conducted on shielded 30kN standard Meyes creep machines with automatic levelling devices. The lever ratio is regularly checked. For the force range in the present test campaign the lever ratio is within 0.7% from the nominal value. A split three-zone furnace, with individual temperature control of each section, was used to heat the specimens to 550°C. The temperature of the specimens is continuously measured with a K-type thermocouple attached to the centre of the creep specimen and two thermocouples attached to the rims of the specimen. The elongation is measured with dual extensometers attached to the small ribs on both of the ends of the gauge length. The displacement transducers are (remotely) calibrated before each test.

The procedure described by R. Bestwick [16] was used to optimise the testing time for creep testing. The Larson-Miller parameter for each of the material conditions (XW, WM, L and T) was updated after each test result. A testing temperature of 550°C, which is the expected accidental/off-normal vessel temperature of the HTR, was chosen for 4 specimens of each material condition.

2.2.3 Impact testing

For the reference testing an instrumented 300J Instron PW 30 Impact Testing Hammer has been used at the JRC.IE laboratories for the CVN specimens, and a smaller Instron PW 5 (50 J) Impact Testing Hammer has been used for testing miniaturized Charpy V-notch samples (KLST). The specimens were climatised for 15 min in a conditioning chamber. The test pieces were transported in a special jig to the anvil and tested well within 5 seconds. The impact velocity was 5.52 m/s for the 300J hammer and 3.85 m/s for the 50J hammer. An instrumented ISO tub has been used. The test method follows the ASTM E23-96 standard and for the instrumented test method the norm ISO/CD 14556 has been used. Calibration of the Impact testing equipment was performed according to the norm NEN-EN 10045-2. The impact energy reading from the dial was compared with the calculated energy from the instrumented data and the deviations were marginal in practically all cases. The biggest single difference observed was 0.31%.

A small Instron-Wolpert pendulum machine installed in a lead shielded hot cell with a maximum capacity of 50 J is used to test the sub-size impact specimens (KLST type). The impact hammer has a speed of 3.85 m/s at impact and is equipped with an instrumented DIN striking edge. The testing practice and analysis is in accordance with the ISO CD14556:2000(E) standard. During the test a specimen is heated up or cooled down to the test temperature and acclimatised for about 30 min (in air or nitrogen) in the conditioning chamber. The test pieces are transported to the anvil and tested within 3 seconds, according to the standards. The actual test temperature is corrected for temperature loss, reproduced with a spot-welded thermocouple on a KLST specimen at 50° intervals.

For each specimen the dial energy and the lateral expansion is noted and the instrumented data from the pendulum machine (i.e. energy, load and displacement versus time) is recorded. From the impact data, the dial energy has been plotted versus the test temperature. The data was fitted using a tan-hyperbolic function: $E=((E_{use}+E_{lse})/2)+((E_{use}-E_{lse})/2)*\tanh((T-DBTT)/r)$ using the lower shelf energy E_{LSE}, the upper shelf energy E_{USE}, transition temperature (DBTT) and shape factor r as fitting parameters. E and T are the measured impact energy and temperature respectively. Occasionally, when the fitted lower shelf energy is negative, the E_{LSE} is kept constant at the lowest value measured, and the data was refitted. Since a decrease in impact energy is expected at higher temperatures (>> DBTT), the data points well above the transition temperature were excluded from the fit. The reported values are the fitted parameters from the tan-hyperbolic function.

In general, the impact energy is dependent on the size and geometry of the impact specimens. However, it is expected that the change or difference in impact properties follows the same trend for all specimen types.

2.2.4 Fracture Toughness testing

The fracture toughness is tested using an Instron servo-hydraulic mechanical testing machine in a lead shielded hot cell. The displacement is measured by an averaging load-line displacement bridge mounted to the CT specimen (with two LDVT's) and the crack growth is monitored using Direct Current Potential Drop (DCPD). The fracture toughness test is performed in accordance with the ESIS P2-92 procedure. The CT-specimens were first pre-cracked by fatigue (decreasing ΔK method) to an $a/W = 0.6$ before irradiation. The specimens were then side grooved (both sides with 10% of the thickness and a top angle of 60°) to avoid severe plastic deformation at the sides of the specimens during fracture testing due to the high expected ductility. At the start of the test the DCPD signal is reset to zero and during loading the DCPD signal, the load-line displacement and the load are simultaneously recorded. After the fracture toughness test the CT specimen is heat tinted and then broken by fatigue to measure the final crack propagation and the actual length of the pre-crack by a nine points average.

From the recorded data, the J-Δa curves are constructed. The energy J during crack blunting stage for small Δa can be described by:

$$\Delta a = 0.4\, d_n^* \frac{J}{E} \tag{1}$$

where d^*_n is a constant depending on the materials tensile properties. It is assumed that the DCPD signal after crack blunting is linearly dependent on the crack extension Δa normalised to the final crack extension. At each temperature two test pieces were used, one with a relative short (0.5 mm) and one with a long crack extension (1.5 mm) in order to verify the crack initiation point.

The data of the individual specimens is fitted with a simple power law fit, as indicated in equation

$$J = A\, \Delta a^b \tag{2}$$

with A the power law constant and b the power law exponent.

The materials were tested at room temperature and 375 °C, the minimum HTR vessel operating temperature. The speed of the crosshead was kept constant and was approximately 0.005 mm/s.

Due to the very high ductility of the mod. 9Cr. steel, the toughness values are specimen size/geometry depended. Therefore the reported toughness values, J_Q and $J_{0.2BL}$ are only valid for specimen thickness of B=10 mm, see also section 4.4.

3 HFR Irradiation of 9Cr. steel

The LYRA irradiation, designed by JRC.IE [18], in the frame HTR-m of has been performed in the Pool Side Facility (PSF) of the HFR position 10 and 11 as shown in figure 2. The PSF irradiation takes place outside the reactor core. Therefore lateral flux gradients are expected within the irradiation rig. The LYRA-08 has been irradiated for two successive irradiation cycles. Only parts of the two cycles have been used by placing the rig at the core box wall when the reactor was already at full power. In-between the two cycles the irradiation rig was turned for 180° to obtain low lateral dose gradients between the specimens. The total irradiation time was 18.2 full power days in PSF position 10&11. A typical cross-section of the capsule is also shown in figure 2.

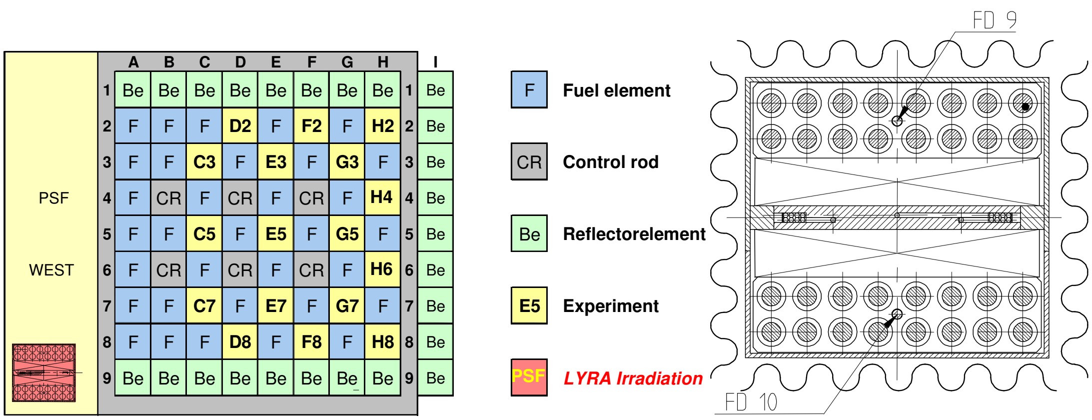

figure 2 Position of the LYRA irradiation inside the HFR and a typical cross-section of the irradiation rig.

The irradiation is monitored and controlled with regard to temperature. The heating sources of this particular irradiation rig are external heaters in addition to the gamma heating of the specimens and capsule. To reduce the amount of gamma heating, a tungsten gamma shield is mounted between the irradiation capsule and the core box wall. The capsule is filled with a mixture of He and Ne gas, which influences through the thermal conductivity of the gas the operation temperature of the sample holder. The temperature is controlled by the external heaters, equipped with 48 thermocouples, and by the distance of the rig from the core box. The heater is split in three sections, which are controlled separately. Therefore, the buckling of the gamma heating can be compensated for by the different heaters.

Typically, a LYRA irradiation capsule has 24 thermocouples mounted inside the rig. The temperatures have been measured at different levels (heights) inside the capsule, mainly near the centres of the tensile specimens or near the notches of the CT specimens. Since external heaters are used to control the temperatures the temperature gradients are small, typically ±13°C. The entire history (every 10 second) of the heat profile over any sample holder is recorded with good certainty. The non-instrumented specimen's temperatures are interpolated from the ~20 calibration points available.

To reach a temperature of ~375 °C a gas mixture of 40% Helium and 60% Neon has been employed. In addition the top, bottom, north, south, and west heaters have been used as a help to maintain the irradiation temperature. In case of too high sample temperature the experiment has to be manually withdrawn from the core box wall. The temperature limit for such an action is set at 385 °C for the sample holder thermocouple readings [19].

The temperature inside the capsule increases due to gamma heating when the capsule is moved towards the core box. The final irradiation temperature is set by the external heaters. The irradiation is considered to be started when the distance to the core box is small, such that the fast fluence rate exceeds a threshold level of approx. $2 \cdot 10^{16}$ $m^{-2}s^{-1}$ (E>0.1MeV). The average irradiation temperatures have been calculated for reactor power P_{HFR}>40 MW to excluded power reductions [19]. The average temperatures, maximum temperatures and the standard deviation of the temperatures are given in table 2 for each vertical level separately. The vertical position of the thermocouples are shown in figure 31, see also figure 49 in appendix G. The average temperature over all thermocouples during the two irradiation cycles is given in figure 31 in appendix B. The maximum occurred at the beginning of the irradiation due to the tuning of heaters and trolley position. The average temperature in the entire capsule was 370°C with a standard deviation of 13°C. The maximum temperature observed was 389°C. It should be mentioned that the average temperatures at the lower part of the irradiation capsule are slightly lower than at the upper part of the capsule.

table 2 Average irradiation temperature for the different vertical positions

Level with respect to centre line core (mm)	Thermocouples	Average temperature (°C)	Standard deviation (°C)	Maximum temperature (°C)
111.5	TC 23/24	375	12	389
73.5	TC 21/22/23	371	11	384
23.5	TC 17/18/19	372	12	382
-18.0	TC 14/15/16	372	12	380
-50.0	TC 11/12/13	372	12	382
-82.0	TC 9/10	369	12	381
-118.5	TC 6/7/8	366	12	380
-162.0	TC 3/4/5	363	12	380
-204.5	TC 1/2	365	13	384

Neutron monitoring is extensive on all of NRG's irradiation experiments. For the LYRA experiment 12 activation monitor sets consisting of various high purity metallic strips are placed at strategic positions within the sample holder. The actual neutron spectrum of the HFR in the irradiation positions is very well known (By detailed MCNP analysis, previous experiments and special flux analysis of HFR). The post-irradiation measurements on the activation sets are used to calibrate/scale the flux profile. The uncertainty of the neutron calculations is 7% for the fast

fluence, 7% for the thermal fluence, and 14% for the number of displacements (dpa), the latter is also due to the uncertainties in damage cross-sections. The individual dose per specimen is interpolated from the 12 activation monitor sets for the thermal and fast fluences. The average fluence of the HTR-m specimens is $9.44 \cdot 10^{22}$ m^{-2} (E>0.1MeV), $3.85 \cdot 10^{22}$ m^{-2} (E>1.0MeV), which gives a dose level for 9Cr steel of 5.84 mdpa. The maximum and minimum fluence are $11.41 \cdot 10^{22}$ m^{-2} (E>0.1MeV), $4.65 \cdot 10^{22}$ m^{-2} (E>1.0MeV), 7.07 mdpa and $7.97 \cdot 10^{22}$ m^{-2} (E>0.1MeV), $3.24 \cdot 10^{22}$ m^{-2} (E>1.0MeV), 4.93 mdpa, respectively. The fluence and dose levels for each individual specimen are reported in table 8 to table 15.
The activation of the mod. 9Cr steel has been calculated for the LYRA irradiation using FISPACT and was reported in [20]. The calculated radioactivity (conservative assumptions) of the specimens amounts after 500 days after the end of irradiation to about 31 GBq/kg, see figure 3. The measured cobalt fluence at the centreline of the experiment (i.e. max fluence) is $2.4 \cdot 10^{22}$ m^{-2}.

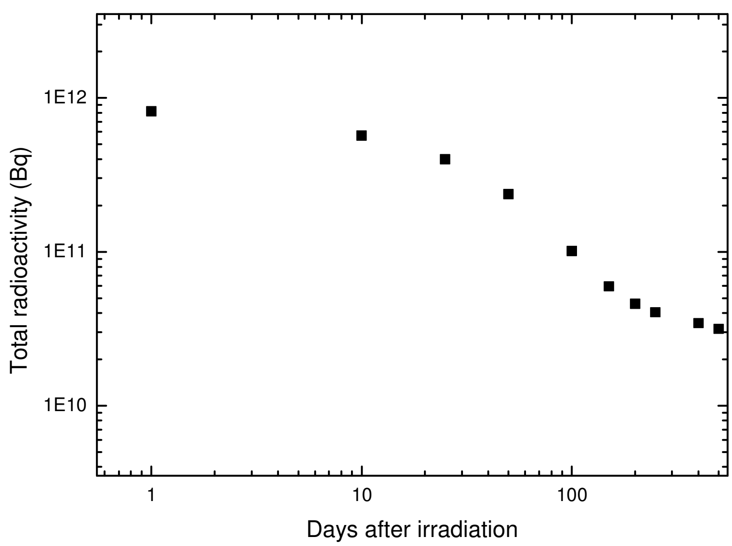

figure 3 Estimated maximum radioactivity levels after the LYRA irradiation [20]

The detailed loading and stacking of the specimens inside the LYRA irradiation is presented in figure 49, appendix G and in [12]. Identical specimens are placed in comparable vertical positions with respect to the centre-line core to minimise fluence gradients effects in the test results.

4 Results

4.1 Tensile tests on mod. 9Cr steel

The tensile tests on the irradiated specimens have been performed at room temperature and 375°C, 450°C and at 550°C. The latter three temperatures are the irradiation temperature c.q. lower vessel operating temperature, the maximum vessel operating temperature and the accident temperature c.q. creep temperature respectively. At this stage of the project no unirradiated data other than room temperature tensile data were available from JRC.IE for comparison with the irradiated material. However, two additional reference tensile tests (base-metal in L orientation) have been performed at 550°C by NRG in the same facility as used for the irradiated tensile specimens. Also a comparison can be made with 9Cr steel from other programmes such as the SPIRE programme on ADS window materials [13].

In figure 4, typical tensile curves are shown for the irradiated mod. 9Cr base metal in L-direction including reference curves at room temperature and 550°C. The insert shows a close-up of the stress-stain curves at RT and 550°C close to the yield point. It should be noted that the reported strain is the plastic engineering strain. From the figure it can be seen that for increasing temperature, the yield strength and the ultimate tensile strength are decreasing. The results of the tensile tests are listed in table 8 and table 9 in appendix C. A yield drop with subsequent strain hardening is observed at room temperature for the irradiated tensile tests. This yield drop is not observed at 375˚C and higher temperatures.

In figure 1, a slight increase of yield strength at room temperature is observed after irradiation. At 550°C no increase of yield strength is noted, but it should be mentioned that the testing temperature in this case is well above irradiation temperature of 375°C, and irradiation induced defects might be annealed.

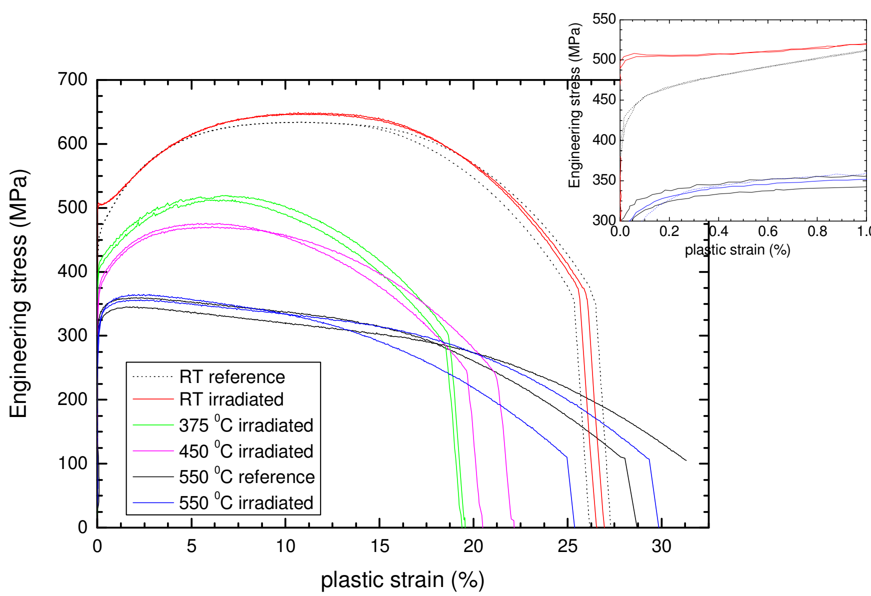

figure 4 Tensile curves from irradiated mod. 9Cr base metal in L-orientation, including irradiated and reference data. Inserted a close-up of the curves close to the yield point.

Figure 5 shows tensile curves at room temperature for irradiated specimens from the mod. 9Cr welded joint. Though the yield strength and ultimate tensile strength of the different material conditions are almost equivalent, a difference in ductility is observed, see also table 8 and table 9. This is more evident in figure 7 where the uniform and fracture elongation are plotted versus temperature.

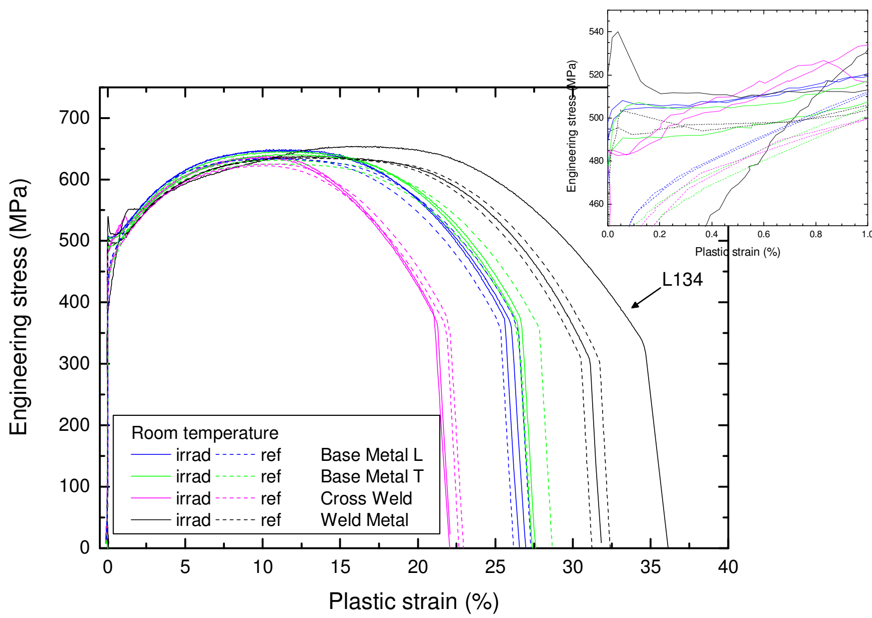

figure 5 Uni-axial stress-strain curves at RT temperature of reference and irradiated mod. 9Cr. welded joint: weld-metal, cross-weld and base metal in L and T orientation.

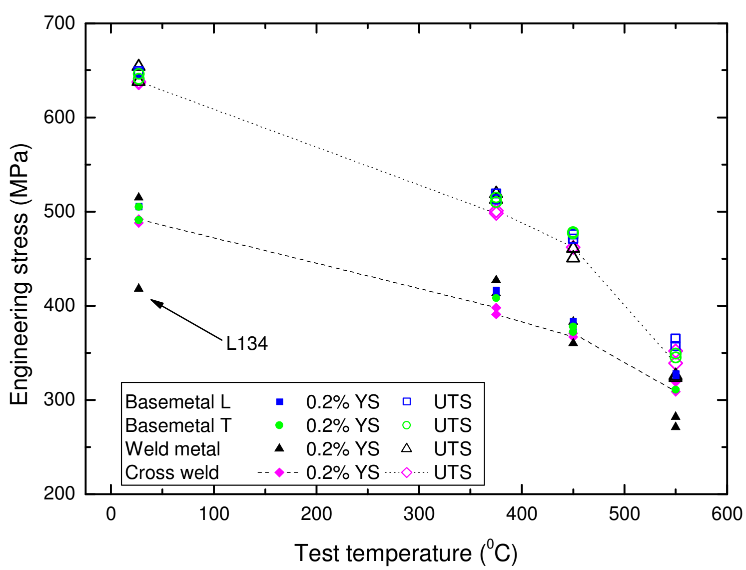

figure 6 Yield strength and ultimate tensile strength versus temperature for irradiated mod. 9Cr for various material conditions.

The yield strength and ultimate tensile strength are plotted in figure 6 versus temperature. Almost no difference in strength is observed between the different material conditions: cross-weld, weld-metal and base metal, showing that an effective PWHT has been applied. The difference between UTS and YS is reduced with increasing temperature and the absolute strength is strongly reduced between 450°C and 550°C. One exception is specimen L134 that was taken from the weld metal from a different plate compared to the other full weld specimens, i.e. plate 4 instead plate 5 and 6 and hence closer to the root of the thick welded joint. This indicates that the properties over the weld show significant variation.

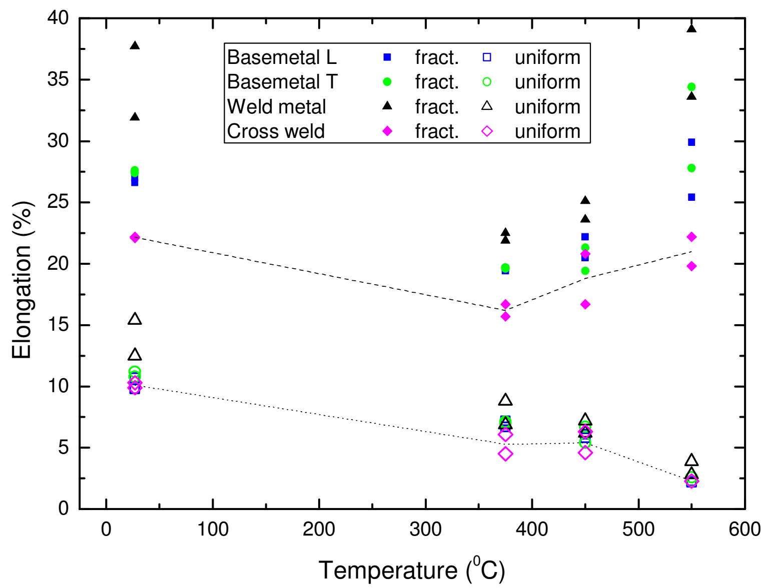

figure 7 Uniform and fracture elongation of the tensile tests of irradiated mod. 9Cr.

Although the weld metal reference data at 375°, 450°C and 550°C is not available, there is a proof that the yield strength hardening at the current dose levels is small for the mod. 9Cr welded joint, i.e. in the order of 40 MPa at room temperature. A reduction of ductility due to irradiation is not observed. The weldmetal has the highest ductility while the cross-weld specimens exhibit the lowest ductility.

In comparison with previous programmes [13], the mod. 9Cr steel has a similar strength at room temperature as EM10. However, comparing with other variants of 9Cr steel, like Eurofer (9Cr2WVTa) and T91, the HTR modified 9Cr steel is somewhat weaker. However, at 550°C the strength is more close to the other 9Cr variants, except for the weld-metal which lies about 25 MPa below the minimum values of the martensitic steels tested in the ADS-programme. But, it needs to be mentioned that at 550°C, the low dose irradiated mod. 9Cr steels are compared here with reference data of other 9Cr. variants.

4.2 Creep experiments on mod. 9Cr steel

The creep tests on mod. 9 Cr steel have been performed at 550°C for nominal rupture times of 100, 300, 1000 and 3000 hrs. The results are shown in figure 8 to figure 14 and the individual creep curves are shown in figure 33 to figure 36 in appendix D on a logarithmic time scale. Please note that the test stresses have not been identical between the reference tests and the irradiated tests as the test stresses have been chosen such that the nominal testing times would be obtained. The times to a strain have been obtained by interpolating between two individual readings, one before and the next after reaching the strain value in question. In figure 9 and figure 10 it can be seen that the behaviour of XW and WM comes closer together when going to higher strain. The same behaviour can be observed for BM-L and BM-T.

The minimum strain rate was determined in a semi-automatic way by selecting a linear part of the strain curve and fitting a linear regression line through these data points and then manually adjusting the data limits such that a good agreement was obtained between the curve and the fitted line.

Note that for the irradiated specimens the failure strain value in figure 13 is the last measurement during the test before failure. The measurement of the failure strain and reduction of area is not possible in the hot cell. Even for the un-irradiated specimens the measurement was difficult as the diameter of the necking area was just above 1 mm and it was extremely difficult to place the broken specimen halves back together. This was done under a microscope, see ... to ... in appendix E. Like expected, due to the concentration of strain in the weakest region, the failure strains of the un-irradiated XW specimens were systematically lower than in the homogeneous specimens (figure 13). In the reduction of area values there was no systematic difference between the four different material conditions.

The Norton exponent and coefficient for the un-irradiated materials were determined from the fitted curves in figure 12. Similarly the stress-rupture exponent and coefficient were determined by plotting the figure 14 with reversed axis and fitting the exponential trend lines for each material. The results have been tabulated in table 3. Similar values will be determined for the irradiated tests when these are completed. It must be noted that a data set of only four tests is not sufficient for a reliable determination of the creep exponents and the corresponding coefficients. At least six data points would be needed and preferably more. Also it is better to determine the coefficients for irradiated and un-irradiated materials separately in order to avoid bias due to differences in testing times.

It can be seen that the exponents for WM in table 3 are considerably higher than for the BM. Although the XW specimen is a “compound” of WM and BM, the exponents for the XW don’t have a specific meaning as the failure location has changed from WM to IC-HAZ. Also the minimum creep rate in a XW test is not a mean value of these two constituents, but an unknown combination of creep rates in WM, BM and IC-HAZ, the proportion of which has changed as a function of the test initial stress. Many test laboratories actually don't even bother measuring the strain in a XW creep test.

The following general conclusions can be drawn on the basis of the results:
1) The results for the base material orientations T and L are almost identical with the transverse direction being slightly weaker (figure 8 to figure 12).
2) The results for the cross-weld and weld metal tests are almost identical with the cross-weld tests featuring shorter times to rupture (figure 8), but longer times to strain (figure 9&figure 10) and lower minimum strain rates (figure 12).
3) Weld metal is weaker than the base material (figure 8 and figure 12)
4) For the base material and the weld-metal the difference between the un-irradiated reference tests and the irradiated tests is almost negligible as all results fall within a very narrow scatter band (figure 8 to figure 12).
5) The only systematic influence of the irradiation can be seen in the cross-weld tests where the testing times are systematically longer (figure 8) and the minimum strain rates are lower (figure 12).
6) The failure location of the unirradiated creep tests for the cross-weld specimens was in the weld metal for times below 1000h. Above this value the failure occurred in the intercritical zone of the HAZ in the base metal (appendix E). In creep testing of ferritic cross-weld specimens it is often observed that the failure at short times is in the weaker of the two (WM or BM), but at longer times the failure is shifted to the HAZ, the shift occurring somewhere between 1000 and 10.000h.
7) As an overall summary of the creep tests it can be stated that the irradiation did not have adverse effects on the creep properties of the materials tested. However, the increase of creep strength in the cross-weld tests after irradiation was unexpected and cannot be explained at the moment.

table 3 Creep exponents for the unirradiated creep tests

	Norton coefficient	Norton exponent	Stress-rupture coefficient	Stress-rupture exponent
BM-L	5.46E-37	14.84	3.67E+35	14.24
BM-T	2.25E-36	14.64	1.59E+35	14.15
XW	2.20E-44	18.25	5.74E+38	15.84
WM	1.51E-43	17.92	9.71E+40	16.77

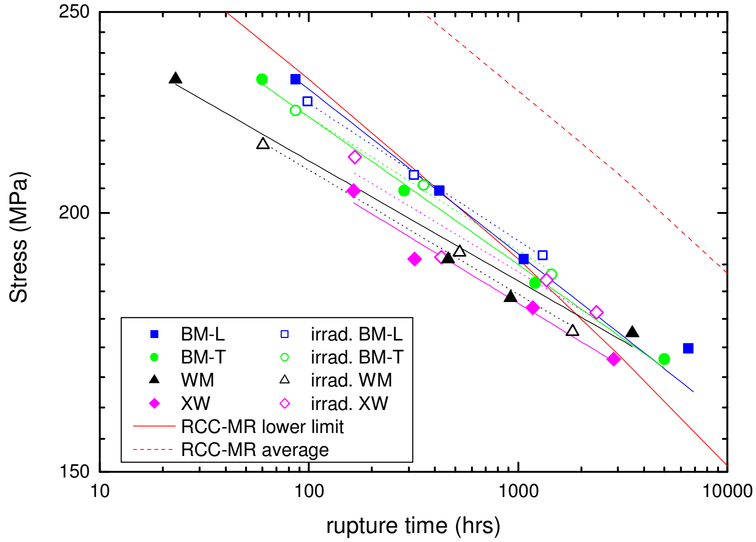

figure 8 Stress-rupture plot of the base material results in transverse and longitudinal direction, the cross weld and weld metal results The trend lines are based on the un-irradiated data.

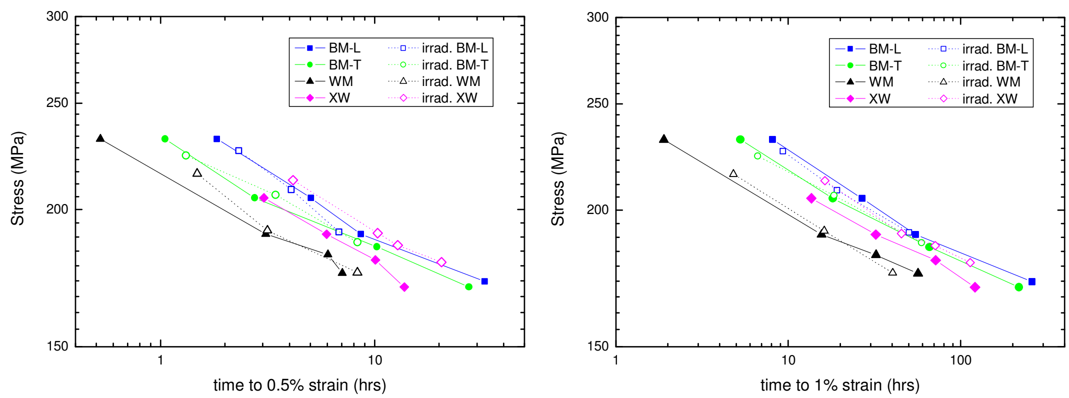

figure 9 Time to 0.5% strain versus stress and right: time to 1% strain versus stress.

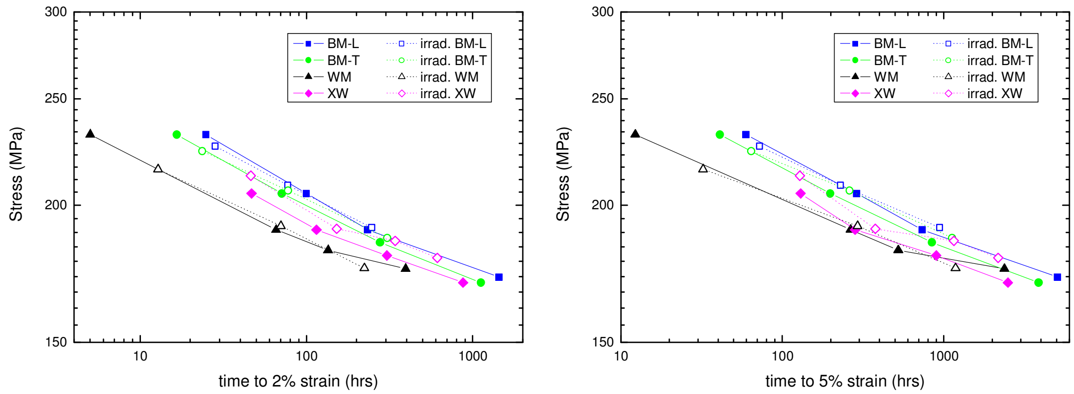

figure 10 Time to 2% strain versus stress and right: time to 5% strain versus stress.

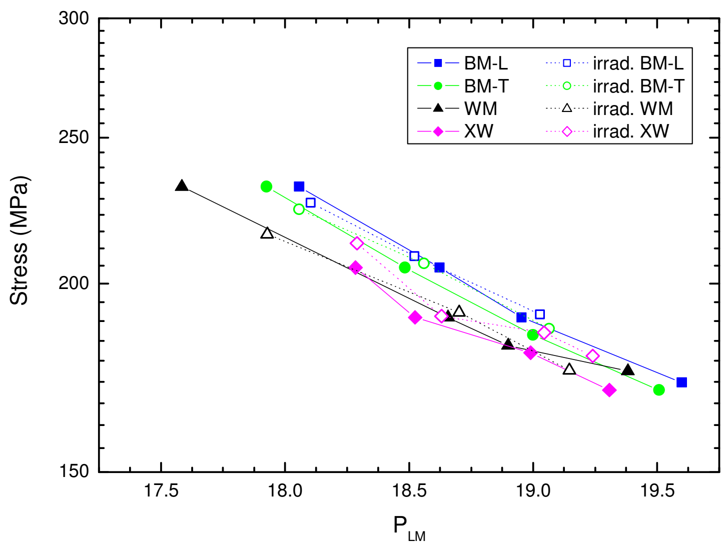

figure 11 Larsson-Miller plot for the base material, the cross weld and weld metal creep tests, showing a slightly different trend between the BM and the welded materials.

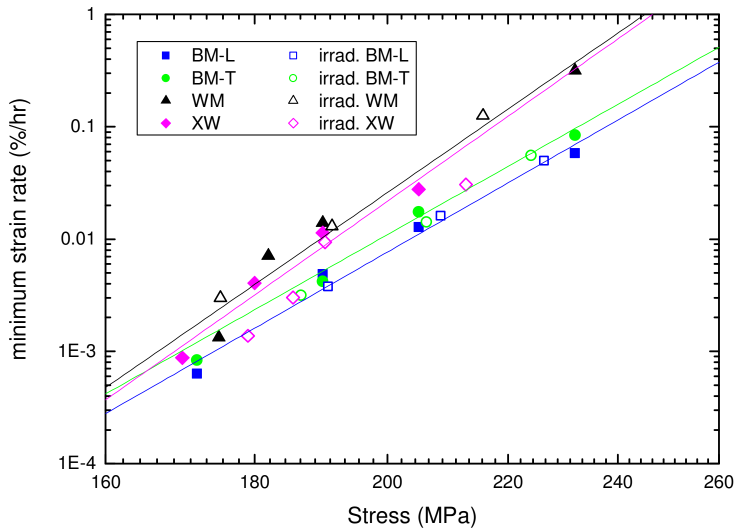

figure 12 Minimum strain rate for the base material and welded materials creep tests, showing a slightly different trend between the BM and the welded materials.

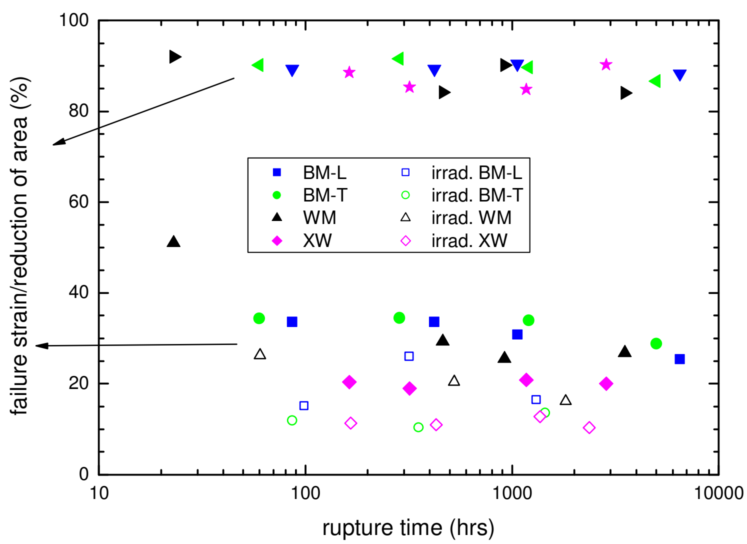

figure 13 Failure strain and reduction of area as a function of failure time. Note that for the irradiated specimens the failure strain value is the last measurement before failure. The measurement of the failure strain and reduction of the area was not possible in the hot cell.

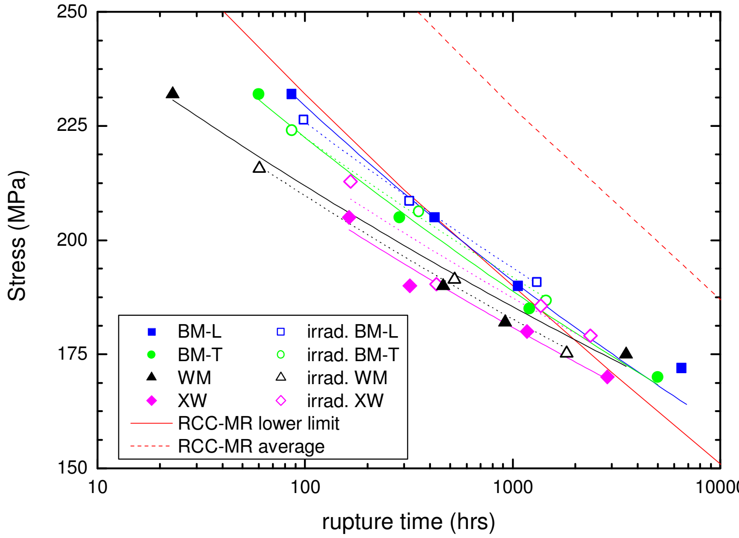

figure 14 Plot of stress rupture results with a linear stress axis (same data as in figure 8).

4.3 Impact tests on mod. 9Cr steel

Impact properties were determined using sub-size and full-size specimens in reference and irradiated condition. Four material conditions were selected (weld metal WM, Heat affected Zone (HAZ) and base metal in two directions, L-T and T-L). The individual data for the impact tests of the sub-size specimens are reported in table 11, table 12 and table 13 in appendix C. The data for the full-size specimens is listed in table 14 in appendix C.

In figure 15 to figure 22 the individual impact results of the sub-size specimens are plotted for both the impact energy and the lateral expansion. The curves in the graphs are fitted using the procedure described in section 2.2.3. The black and green dots and lines are the pre-irradiation results while the blue and red dots and curves are for the irradiated specimens. The dotted lines are used to group the results and to indicate the scatter bands of the impact curves. Because of the gradual decrease of impact energy for test temperatures over 50°C, these results are excluded from the curve fit. Other excluded points, due to large scatter from the impact curve are encircled in red.

In the reference impact tests the lowest ductile to brittle temperature (DBTT) was observed for the heat affected zone and for the weld material. Both plate directions L-T and T-L exhibit a similar DBTT. The weld metal shows beside the lowest DBTT also the highest upper shelf energy, which underlines the high upper shelf fracture toughness for this material as described in section 4.4.

In the same figures, the results of the irradiated specimens are plotted, as well as the fitted curves. The scatter between the irradiated specimens is higher than for the reference material especially at the upper shelf energy due to variation in fluence level; see the dotted bands for the irradiated HAZ and weldmetal specimens. Similar graphs are plotted for the measured lateral expansion. In this case the expansion at the upper shelf and the expansion at the lower shelf are used as fitting parameters instead of the impact energy. The fitted parameters are listed in table 4 and table 5 for the impact energy and the lateral expansion respectively. It should be noted that due to the scattering of the data, the fitting parameters have a large margin of error. However, they do allow estimation of the DBTT at half the USE to give an indication of the shift in transition temperature. Moreover, the change of upper shelf energy as a result of neutron irradiation can be determined.

Table 4 also contains the shift of DBTT and the change of upper shelf energy for the four different material conditions. The shift determined from the lateral expansion and the change of lateral expansion at the upper shelf is reported in table 5. The numbers can only be used as an indication since the shifts are relatively small compared to the scattering. A shift of the ductile to brittle transition temperature to higher temperatures can be observed from both tables. Moreover a significant increase in upper shelf energy was observed of over 20% as indicated in table 4 while the mod. 9Cr steel exhibits a decrease of lateral expansion shown in table 5. This increase of upper shelf energy has also previously been observed for other (commercial) 9Cr. steels [13] and can be explained by an increase in yield strength while the loss of ductility is not significant at this fluence level. The increase in yield strength and lack of decrease of ductility was observed with tensile tests, described in section 4.1. It should be mentioned that the thermal effects like, i.e. thermal aging, during the irradiation at 375°C time of 18.2 days is negligible.

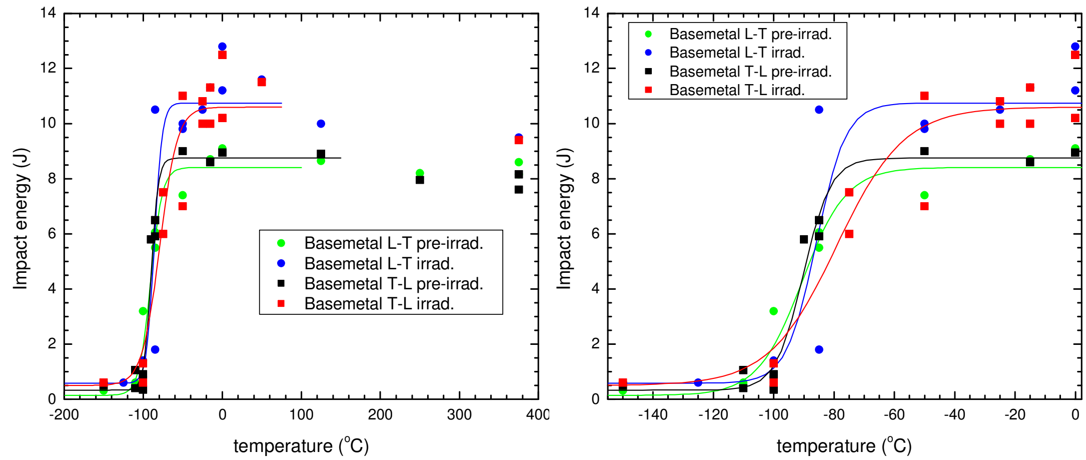

figure 15 Ductile-to-brittle transition curves of the base metal in the T-L and L-T direction for both the reference and irradiation condition and a close up of the transition zone (right)

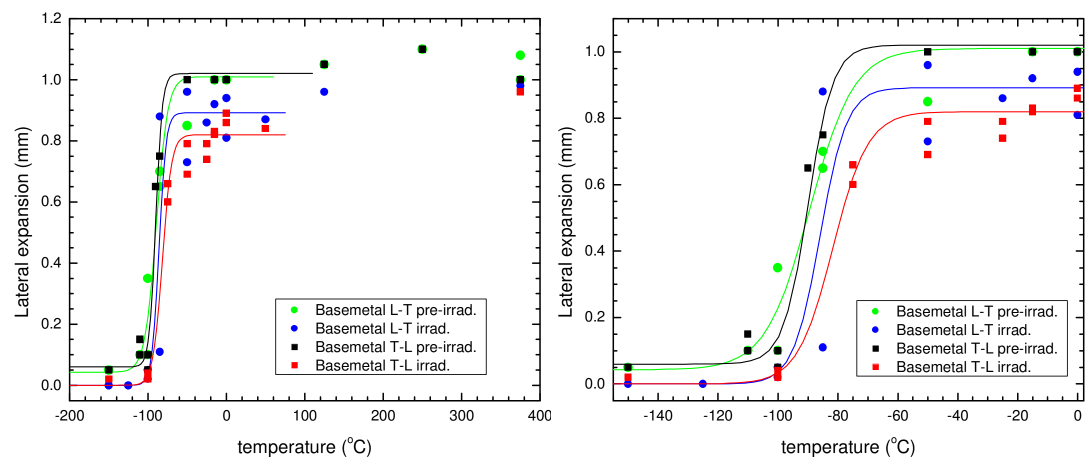

figure 16 Ductile-to-brittle transition curves of the base metal in the T-L and L-T direction for both the reference and irradiation condition in terms of lateral expansion and a close up of the transition zone (right)

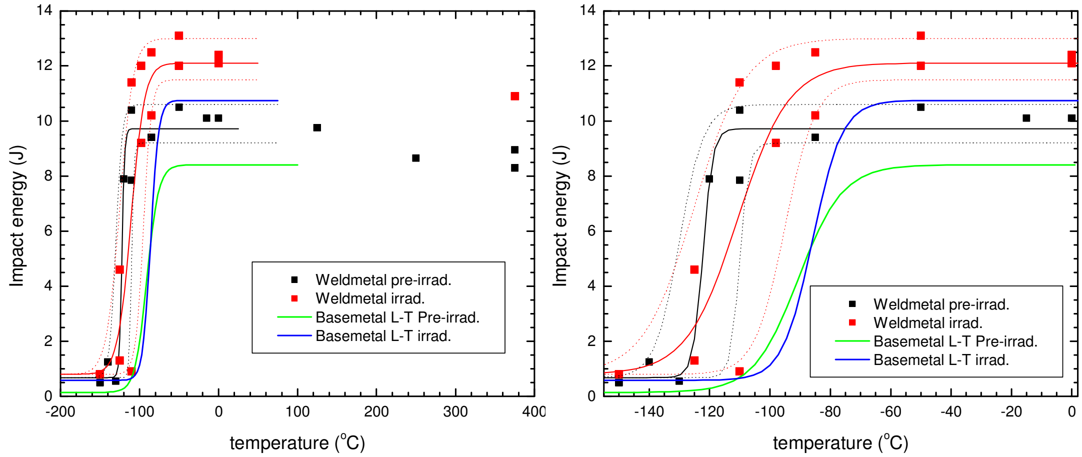

figure 17 Ductile-to-brittle transition curves of the weld metal including the basemetal (L-T) average line for both the reference and irradiation condition and a close up of the transition zone (right)

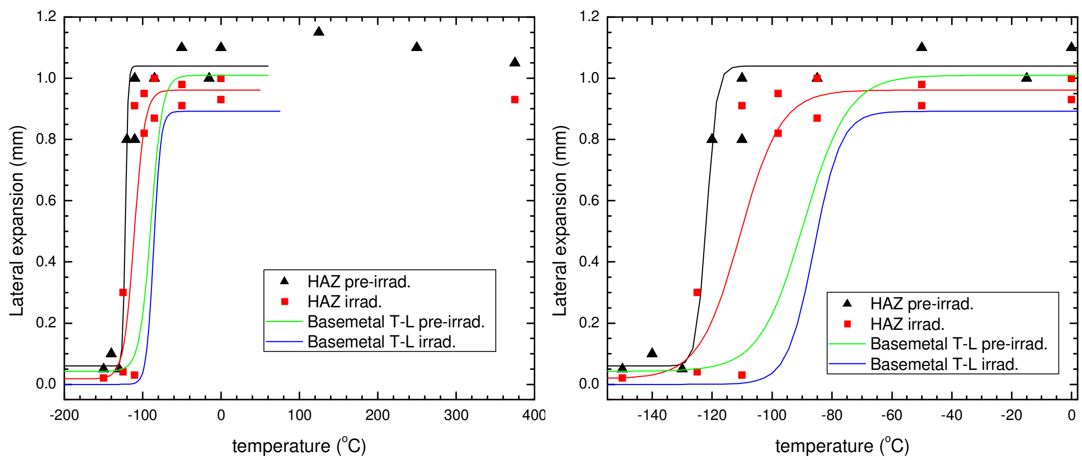

figure 18 Ductile-to-brittle transition curves of the weld metal including the basemetal (L-T) average line for both the reference and irradiation condition in terms of lateral expansion and a close up of the transition zone (right)

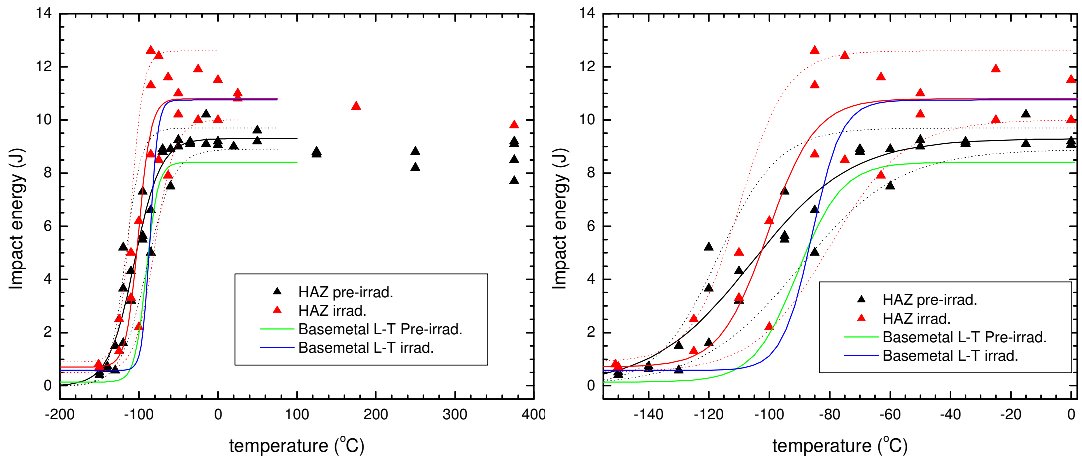

figure 19 Ductile-to-brittle transition curves of the HAZ including the basemetal (L-T) average line for both the reference and irradiation condition and a close up of the transition zone (right)

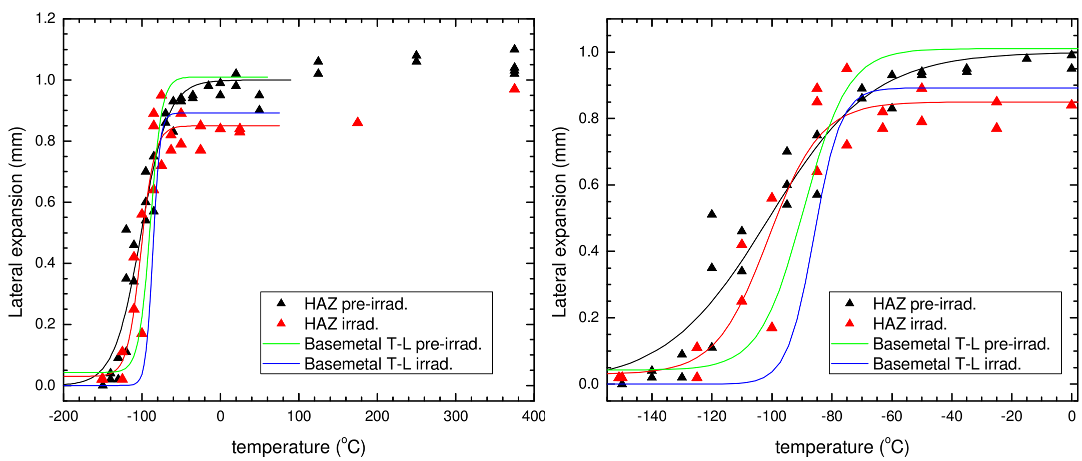

figure 20 Ductile-to-brittle transition curves of the HAZ including the basemetal (L-T) average line for both the reference and irradiation condition in terms of lateral expansion and a close up of the transition zone (right)

table 4 Results of the impact tests on sub-size KLST type specimens using the impact energy.

Material	Pre-irradiation			Irradiated				
	E_{LSE} (J)	E_{USE} (J)	DBTT (ºC)	E_{LSE} (J)	E_{USE} (J)	DBTT (ºC)	ΔDBTT (ºC)	ΔUSE (%)
BM L-T	0.1	8.4	-91	0.6	10.7	-86	5	+27
BM T-L	0.3	8.7	-90	0.0	10.6	-79	12	+26
WM	0.7	9.7	-122	0.8	12.1	-111	11	+25
HAZ	0.0	9.0	-106	0.7	10.8	-101	5	+19

table 5	Results of the impact tests using on sub-size KLST type specimens the lateral expansion.

material	Pre-irradiation			Irradiated				
	LE_{LSE} (mm)	LE_{USE} (mm)	DBTT (ºC)	LE_{LSE} (mm)	LE_{USE} (mm)	DBTT (ºC)	ΔDBTT (ºC)	ΔLE_{USE} (%)
BM L-T	0.04	1.01	-89	0.01	0.89	-86	3	-12
BM T-L	0.06	1.02	-90	0.00	0.82	-82	8	-20
WM	0.06	1.04	-122	0.02	0.96	-111	11	-8
HAZ	0.0	1.00	-101	0.03	0.85	-101	0	-15

Full-size charpy specimens have been included to study the specimen size effect. Only three material conditions have been selected. For two material conditions, weld metal and base metal in T-L direction, sufficient number of specimens were available to cover the full transition curved, while for the Heat Affected Zone (HAZ) only 2 specimens were available. In figure 21 and figure 22, the results are shown for both the lateral expansion and impact energy. In addition, the fitted tan-hyperbolic and an impression of the scatter band are shown. The impact energy at 375°C could not be determined since the capacity of the testing machine was too low (max. 300 J), therefore the result might be higher. This can also be observed from the lateral expansion, which is lower than expected from the transition curve. The fitting parameters for both, impact energy and lateral expansion are shown in table 6. The DBTT was calculated at half of the upper shelf energy E_{USE}, at 41 J and at 68 J. The DBTT, determined from the lateral expansion, is also given in the table.

table 6	Results of the impact tests of the full-size charpy specimens using the impact energy (J) and the lateral expansion (mm). The transition temperatures are given in ºC

	Impact energy					Lateral expansion		
material	E_{LSE}	E_{USE}	DBTT	$DBTT_{41J}$	$DBTT_{68J}$	LE_{LSE}	LE_{USE}	DBTT
BM T-L	3.8	249	-27	-74	-55	0.10	2.45	-45
WM	4.9	290	-76	-89	-85	0.20	2.5	-79

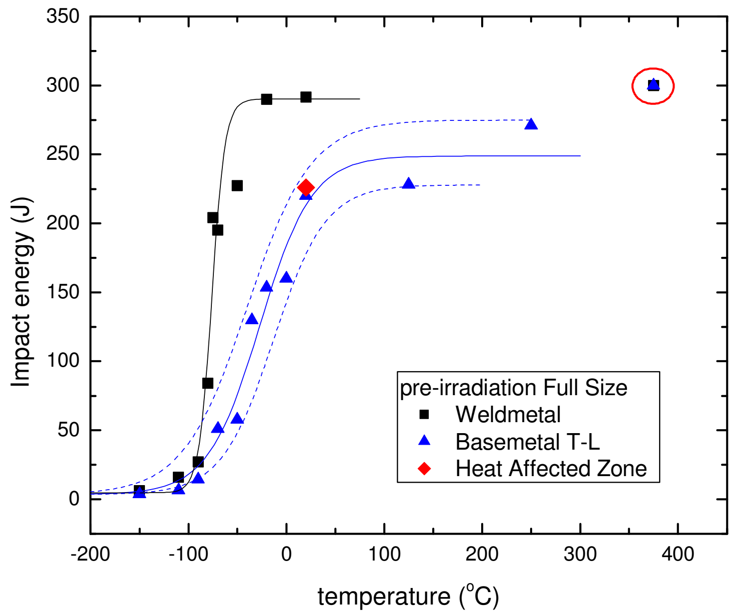

figure 21 Ductile-to-brittle transition curves of the weldmetal and the base metal in T-L direction using full-size charpy specimens in reference condition.

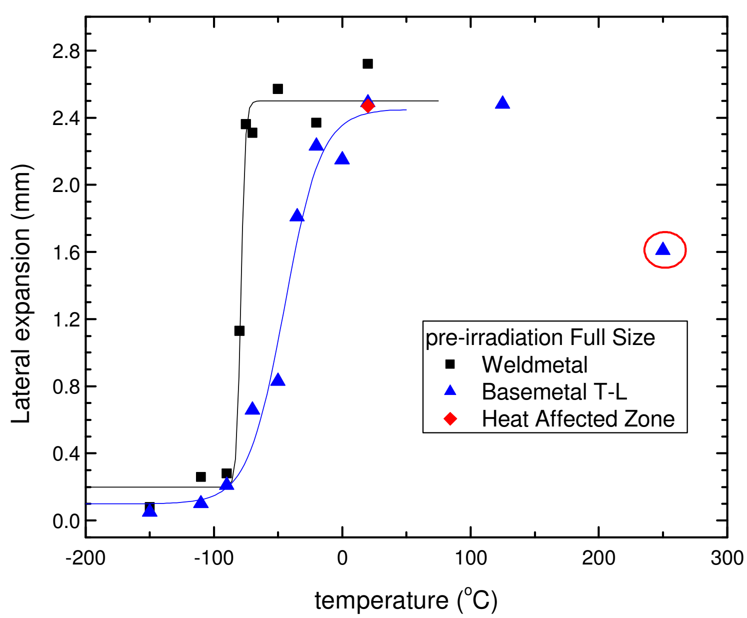

figure 22 Ductile-to-brittle transition curves of the weldmetal and the base metal in T-L direction using full-size charpy specimens in reference condition.

The specimen size effect for impact testing is in general described by [21][22]:

$$E_{USE,\,fullsize} = NF * E_{USE,\,subsize}$$

$$DBTT_{fullsize} = DBTT_{subsize} + C$$

where NF and C are a normalisation factors. For high ductile materials, like the mod. 9Cr steel, with the assumption of nominal fracture volume rather than nominal fracture area, the relation for the scaling factor *NF* is usually written as [21]:

$$NF = \frac{(Bb)^{3/2}\,fullsize}{(Bb)^{3/2}\,subsize}$$

The sub-size impact reference tests that have been carried out on the weld metal and base metal have been scaled to the full-size charpy impact results, shown in figure 23 in terms of impact energy and not corrected in DBTT. The upper shelf energies from table 4 and table 6 have been used to evaluate the scaling factor *NF* for both, the weld metal and base metal. The normalisation constant C has been determined at half of the upper shelf energy. The results are listed in table 7. In addition the factor *NF* calculated from the specimen dimension using the equation above is given. The slightly higher numbers for NF have also been reported before [22].

table 7 Impact normalisation factors for full-size charpy and KLST sub-size impact specimens

Material	***NF***	**C** (°C)
Base metal T-L	28.6	63
Weld metal	29.9	46
Theory	26.5	

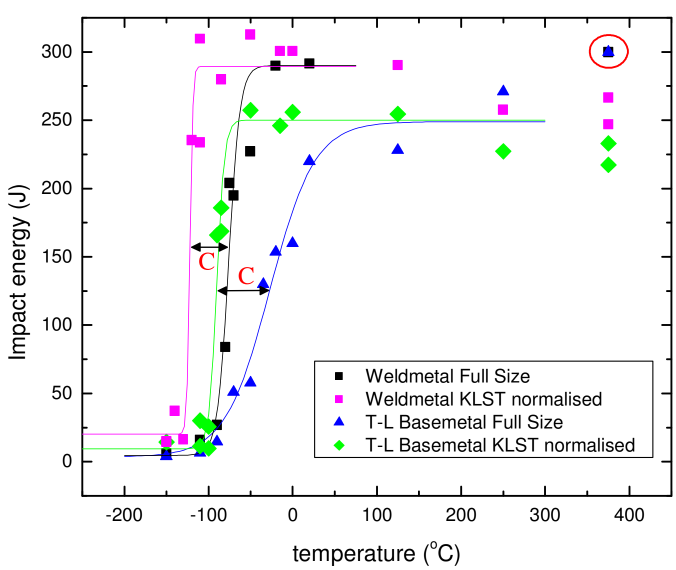

figure 23 Specimen size effect for unirradiated specimens, corrected for upper shelf energy, normalisation factor C is indicated.

4.4 Fracture toughness on 9Cr steel

As described in section 2.1, 2.2.4 and in reference [11], mod. 9Cr specimens have been tested at room temperature and 375°C (irradiation temperature) in various material conditions and orientations namely base metal in L-T and T-L direction, with the notch in the Heat Affect Zone, and with the notch in the full weld metal. In the analysis of the test-data the actual measured tensile data has been used to calculate the full J-R curves. Young's modules of 216 GPa and 199 GPa has been for the fracture toughness tests at room temperature and 375°C, respectively. CT-specimens with a thickness of B = 10 mm, a width of 22.5 mm and a nominal initial crack length of $a_0/W = 0.6$ are used for the fracture toughness tests [11].

At this stage of the project only results of the irradiated fracture toughness tests are available. Therefore no comparison with unirradiated material can be made and therefore the irradiation effect cannot be determined.

The initiation point of the onset of fracture is difficult to determine experimentally due to crack blunting and other effects and therefore the reported curves are considered to be valid from Δa=0.2 mm and up to the maximum crack extension reached during testing. The individual results are given in table 15 in appendix C. In figure 24, the J-R curves are given for the fracture toughness tests at room temperature on the irradiated specimens. From the figure it can be concluded that the toughness of the weld metal is highest, where the heat affected zone has a somewhat lower toughness and both plate direction have similar but the lowest toughness values. The scatter between the individual specimens is largest for the heat-affected zone (HAZ), which can be explained by crack location, either in a coarse grain part or in fine grain HAZ and due to other microstructural variations inside the HAZ. Side grooves have been used to guide the crack to obtain straight crack extensions. In general the reproducibility of the toughness tests are good.

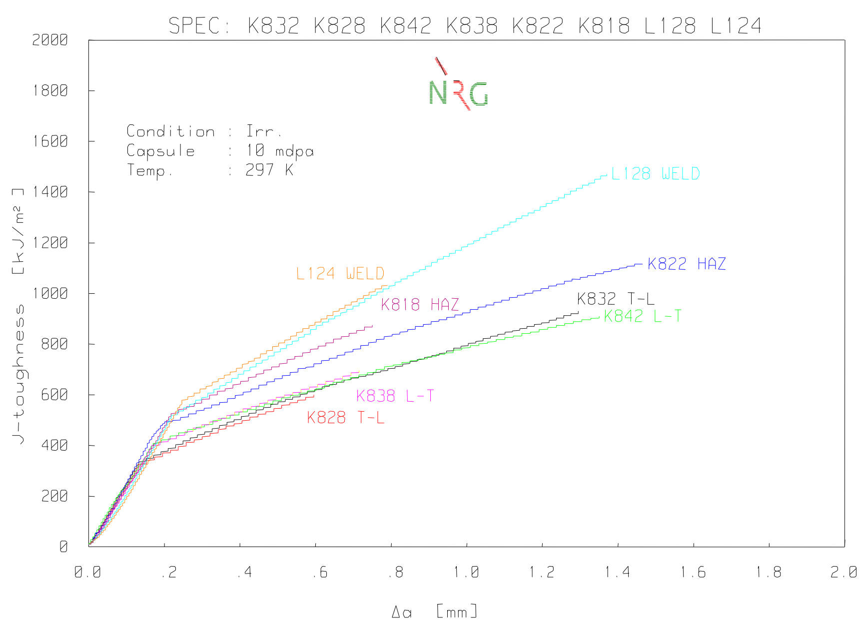

figure 24 raw J-R curves at room temperature of low dose irradiated mod. 9Cr for various material conditions and B=10 mm

The J-R toughness results at 375°C are displayed in figure 25. Also at this temperature the toughness of the weld metal is highest and the toughness of the plate (base metal) lowest. Again the scatter of the J-R curves of the HAZ is relatively high. Compared to the room temperature tests the toughness at 375°C is lower. Figure 26 contains the power-law fitted J-R curves of grouped data for both the RT tests and for the fracture toughness tests at 375°C of the irradiated CR specimens, including the confidence bands. 40 to 50% reduction in the J-R curve is observed going from room temperature to 375°C.

According to the ESIS P2-92 procedure for determining fracture behaviour of materials the maximum J value to obtain geometry independent values can be calculated from the minimum of $J_{max} = (W\text{-}a_0)R_f/20$ and $J_{max} = BR_f/20$ where R_f is the flow strength of the material (ASTM E1820 uses the yield strength $R_{0.2p}$ instead of the flow strength $R_f = (R_{0.2p}+R_m)/2$). For the mod. 9Cr J_{max} is in the order of J_{max} = 260 kJ/m^2 and J_{max} =135 to 155 kJ/m^2 for room temperature and 375°C testing temperature respectively. Small variations in the validity values are due to the variation of strength for the different material conditions. In figure 24 and figure 25, its is clear the the crack initiation is above the maximum J value for all curves, which means that all reported J values are geometry dependent.

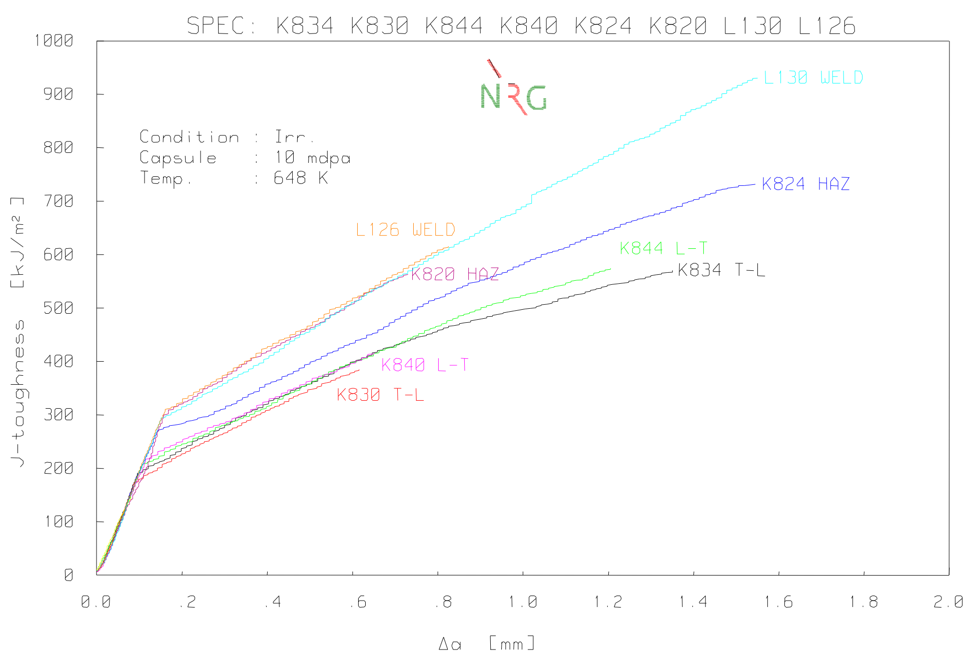

figure 25 raw J-R curves at 375°C of low dose irradiated mod. 9Cr for various material conditions and B=10 mm

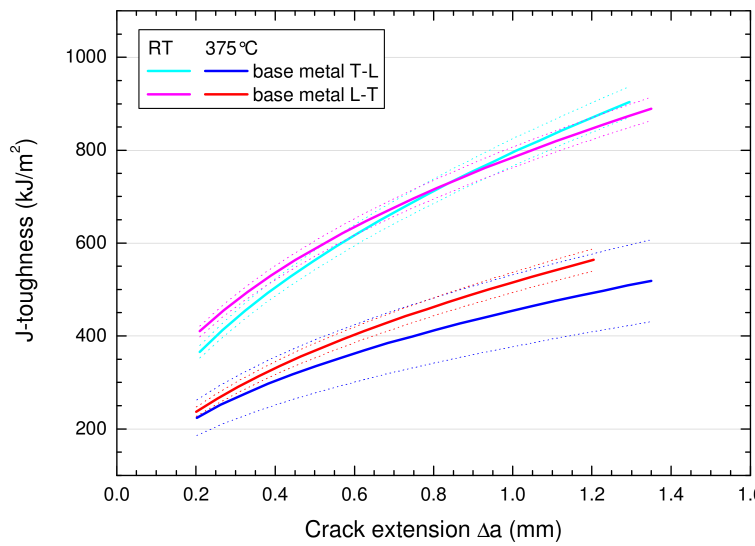

figure 26 Power-law Fitted J-R curves for irradiated basemetal both RT and 375°C fracture toughness tests and B=10 mm

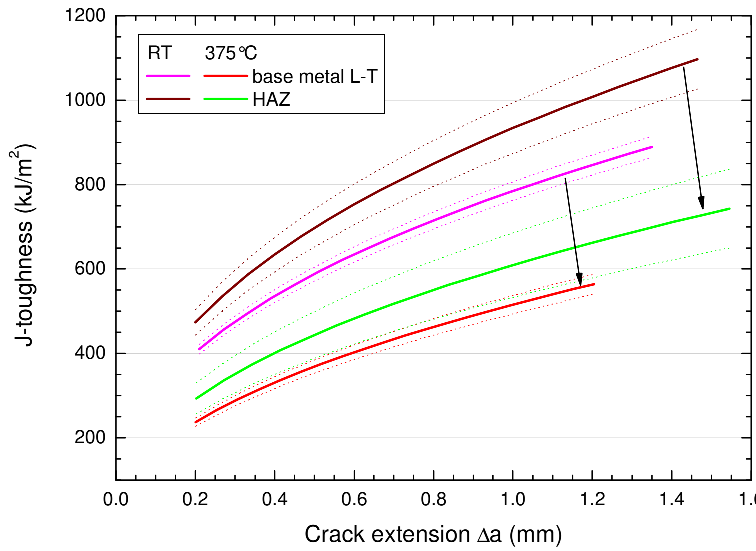

figure 27 Power-law Fitted J-R curves for irradiated HAZ both RT and 375°C fracture toughness tests compared with the basemetal (L-T) and B=10 mm

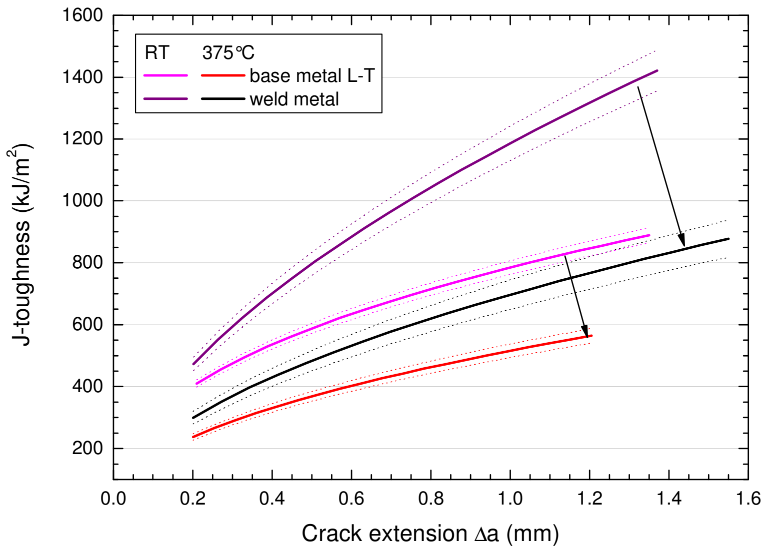

figure 28 Power-law Fitted J-R curves for irradiated weld-metal both RT and 375°C fracture toughness tests compared with the basemetal (L-T) and B=10 mm

Comparing the engineering fracture initiation parameter $J_{0.2\ bl}$,, see table 15, significant higher toughness values are found for irradiated the weld metal (~816 kJ/m^2) with respect to the irradiated base metal (496 to 540 kJ/m^2) at room temperature. The same can be concluded for the toughness tests at 375°C. For comparison, CT specimens of a commercial grade T91 [13] were included. Fracture toughness values for this type of irradiated 9Cr1Mo steel are in the order of $J_{0.2\ bl}$ = 416 kJ/m^2 and $J_{0.2\ bl}$ = 209 kJ/m^2 for room temperature and 375°C tests respectively, i.e. much lower values compared to the mod. 9Cr steel, see figure 29 for a comparison between mod.9Cr base metal and T91

Since no reference tests have been performed on the modified 9Cr steel within the frame of HTR-m programme so far, it is impossible to determine irradiation effects and discriminate them from other effects. However, the current low dose irradiated fracture toughness results of mod. 9Cr show higher toughness values compared to reference fracture toughness values of other 9Cr steels like Eurofer (9Cr2WVTa), EM10, T91, tested in other programmes.

With this comparison no conclusions can be made on the low dose irradiation effects on the fracture toughness of mod. 9Cr of the HTR-m programme!

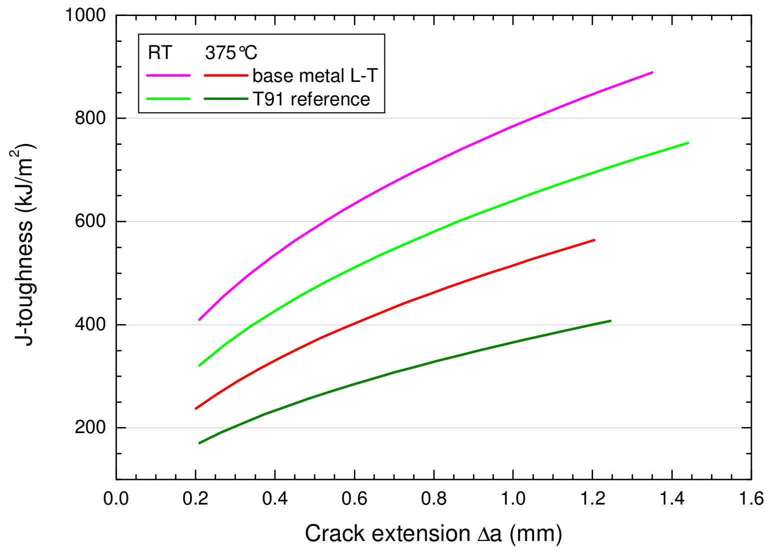

figure 29 Power-law Fitted J-R curves for irradiated weld-metal both RT and 375°C fracture toughness tests compared with the basemetal (L-T) and B=10 mm

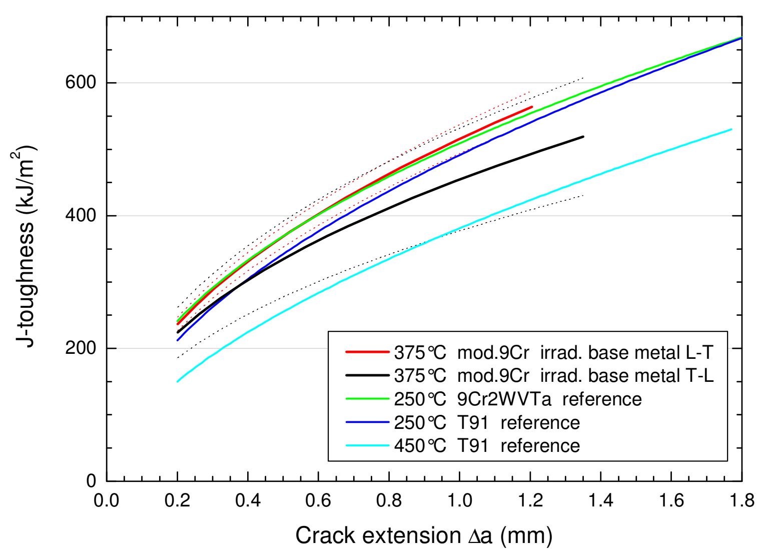

figure 30 Power-law fitted J-R curves of 9Cr steels from the HTR-m programme compared with data from the EU-SPIRE programme for specimen thickness of B=10 mm

5 Discussion

A mod. 9Cr steel was selected as candidate reactor pressure vessel steel for the high temperature reactor for a irradiation testing programme on a thick welded joint. The welded joint was produced by Framatome ANP and had a PWHT optimised for toughness properties. The testing programme comprised tensile, creep, impact and fracture toughness tests.
The tensile tests at room temperature for all material conditions show only a small yield strength hardening ΔYS of about 40MPa while negligible loss of ductility $\Delta\varepsilon_f$ was observed. This is an indication that the mod. 9Cr.steel was over tempered and very soft. A secondary yield drop and subsequent strain hardening was observed for the irradiated tensile tests at room temperature, i.e. well below irradiation temperature, but not at higher testing temperatures on irradiated specimens, nor on the reference tensile tests. This effect may be explained by Cottrell type decoration of dislocations together with defect clusters, which are swept away in the first stage of loading and consequently lowering the tensile stress. At higher testing temperatures, these types of defects disappear.

In creep-rupture tests at 550°C, lower rupture times were observed for the weldmetal and cross-weld specimens on one hand and for both basemetal directions on the other hand in reference and irradiated condition. Also the creep exponent is slightly different which results in larger differences in rupture times at higher stresses. This can be explained over tempered weld metal and by a fine grain HAZ. It should be noted that the heat-treatment was optimised for toughness with a counter effect on creep properties. This is also the reason that the creep-rupture plots might be below (but close) to the minimum RCC-MR design curves for modified 9Cr. The irradiation effect is within the scatter band of creep testing. The irradiation hardening was most clear for the cross-weld specimens. Since the irradiation hardening of both base metal and weld-metal is negligible, the hardening of cross-weld specimens must be explained by irradiation effects in the HAZ.
In tempered martensitic steels, like in all ferritic steels in general, the heat cycle of the welding causes microstructural changes in the base metal next to the fusion line. This heat affected zone (HAZ) is typically 3-4 mm wide. The type and chemical composition of the welding consumable does not have any influence of the width of the HAZ, the only parameter which will influence this is the heat input. (In dissimilar welds the differences in chemical composition, especially chromium content, can cause diffusion of carbon towards the constituent with the higher chromium content, but that is not relevant for the P91 HTR-M weld.) The microstructural changes cannot be avoided because these changes are caused by the heat cycle produced by the welding. The heat of the welding increases the temperature of the base material and the martensitic structure is transformed to austenite, and all the carbides will be dissolved into austenite. When the austenite later cools down it is transformed back to martensitic structure.
Closest to the fusion line the base metal remains solid, but is heated so high in the austenite region that grain growth occurs and therefore the resulting microstructure has very coarse grains. Therefore this zone is named coarse grained HAZ (CG-HAZ). Next to this zone is a region where the metal is heated to a lower austenitic region. No grain growth occurs at this lower temperature

and the result is a fine grained microstructure (FG-HAZ). The width of these two zones is roughly 1mm each and these are the only ones which can be recognised in optical microscopy. In hardness testing the CG-HAZ shows typically values higher than the base material while the FG-HAZ hardness values are same or close to the base metal values.
Further away from the fusion line is a third zone, the "intercritical" zone, which is characterised by the fact that the transformation to austenite has been only partial. As a result of this the pre-existing carbides have not dissolved completely, and when the structure cools down and transforms back ferritic (martensitic) structure, the undissolved carbides act as nucleation sites for the excess carbide in the martensite and as a result there will be large carbides in a matrix which lacks most of the normal fine carbides. The interparticle spacing has grown while the number density has decreased. These changes in carbide structure cannot be seen in optical microscope. A TEM investigation is needed to reveal the nature of the carbide distribution. However, the hardness test will react to the lack of fine carbides as the movement of dislocations has become easier when the fine carbides are not pinning the dislocations. Therefore in a hardess profile across the HAZ the minumum is often found in the IC-HAZ. The width of the intercritical zone is typically 1mm.
In cross-weld tensile testing the weak intercritical zone will not be revealed as it is a narrow soft zone sandwitched between two stronger material (the CG-HAZ especially is stronger than BM). The constraint effect will prevent the soft zone from deforming and therefore the XW tensile specimen normally fail either in base metal or in the weld metal, which ever is weaker. This often leads to the misconception that the weld strength factor (WSF) is 1.0. The situation becomes more complicated when a cross weld specimen is subjected to a creep test. In short term tests (<1000h) the constraint effect is still there and the failure happens either in BM or WM, and then the WSF is still 1.0, but as the stress is lowered and the testing times become longer then there is more time for cavitation to occur in the soft IC-HAZ and indeed this becomes the failure location. The failure times are cut short, and in long term tests above 10.000h the WSF can fall as low as 0.8...0.6. In high temperature plant conditions at long service times (>100.000h) it is typical thet the failure occurs in the IC-HAZ without much deformation of the surrounding material.
What happens to the HAZ during an irradiation is another matter. The HTR-M experiments show that the stress rupture times of the XW specimens after irradiation were systematically longer than those of the unirradiated reference tests. At the moment the authors are not able to explain this observation completely. However in the tensile tests it was observed that the yield strength had increased during irradiation at test temperatures lower than 550'C. It can be speculated that the irradiation might still have had a strengthening effect on the constraint in or around the soft IC-HAZ of the XW creep specimens at 550'C, as the tensile properties in general don't correlate directly with creep properties. Hardness is generally known to correlate more with the microstructure and creep correlates more with the carbide structure.

An increase in upper shelf energy was observed from impact testing after irradiation while negligible shift of transition temperature was noted. This increase of impact toughness can be explained by an increase in yield strength and lack of decrease of ductility. This result is supported by the Room Temperature tensile results where a ΔYS of 40 MPa was observed and no decrease in uniform and total elongation. Therefore the material can absorb more energy before fracture.

Very high fracture toughness results of irradiated mod. 9Cr were observed which underlines the successful post weld heat treatments optimised for fracture toughness. Due to these high toughness values the numbers are geometry dependent, i.e. outside the validity box and therefore only valid for a width of B=10 mm. On the other hand, comparison with available (commercial) reference material indicates that despite neutron irradiation at the current fluence levels of mod. 9Cr, the toughness values are higher than for the commercial 9Cr steels on the same specimen size. A considerable reduction of toughness was observed going from RT to 375°C

Both base metal orientations exhibit similar results for all mechanical tests performed due to the cross rolling of the basemetal. In general, for all material conditions and mechanical tests, the irradiation effect at 375°C at a dose of 5.85 mdpa is small and most likely negligible compared to a batch-to-batch variation. The mechanical behaviour is much better than the commercial T91 from the ADS programme due to impurities and a not optimised microstructure.

6 Conclusions

This report contains the mechanical test data of reference and irradiated mod. 9Cr thick welded joint. The irradiation took place at 375°C for 18.2 days, i.e. the achieved average irradiation fluence was $9.44\cdot10^{22}$ m^{-2} (E>0.1MeV), which is 5.85 mdpa. Subsequently, tensile, creep, impact and fracture toughness tests have been performed under High Temperature Reactor relevant conditions after which a comparison with reference tests was performed. From the test data it was concluded that:

- Although the reference data at 375°, 450°C and 550°C is not available, there is proof that at RT the yield strength hardening at the current dose levels is small for the mod. 9Cr welded joint, i.e. in the order of 40 MPa at room temperature. A reduction of ductility due to irradiation is not observed. The weldmetal has the highest ductility while the cross-weld specimens exhibit the smallest ductility.
- The creep results of the reference tests and irradiated tests are within the same scatter band except for cross-weld specimens which show increase of rupture times with a factor of approx 1.6.
- While negligible shift of ductile to brittle transition temperatures was observed up to ΔDBTT = 12˚C, an increase of 25% of the upper shelf energy was noted. In addition a loss of lateral expansion between 8 to 20% at the upper shelf was observed. The specimen size effect was studied in reference conditions and the scaling factors found are in agreement with previously reported values for 9Cr steels.
- High toughness values, ranging from $J_{0.2bl}$ = 251 kJ/m^2 to 468 kJ/m^2 and $J_{0.2bl}$ = 488 kJ/m^2 to 833 kJ/m^2 at 375˚C and RT respectively, have been measured for the weld metal. From the tested material conditions, the weld-metal has the highest values, while the two base metal orientations have lower toughness values. A reduction of fracture toughness with a factor 40-50% is observed between room temperature tests and FTT tests at 375°C. No conclusions on irradiation effects on fracture toughness can be drawn, since no reference results are available at this moment. The toughness values are size depend and only valid for specimen thickness of B=10 mm.

In general it can be concluded that for the current low irradiation dose, the irradiation effects on mechanical properties are minimal. However, it should be mentioned that the tested welded-joint contained a few hot-cracks, which was attributed to impurities in the filler material. The testing programme was based on specimens taken from part of the welded joint without crack indications.

Literature

[1] R D W Bestwick, *Preliminary review of RPV materials used on HTR and other gas cooled reactors,* NNC Report C6463/TR/004, September 2001, HTR-M-01/9-D-1.1.9

[2] A Buenaventura, *Materials Selection for HTR Pressure Vessel*, Empesarios Agrupados Internacional Document No. 092-089-E-M-00001, Issue 1, 11 October 2001, HTR-M 01/10 D 1.0.17

[3] M T Cabrillat, *HTR-M WP 1.4: Damage Mechanisms*, CEA Document NT-SERI/LCSI/01/4044, Indice 0, 11 February 2002, HTR-M 01/11 D 1.1.18

[4] A Buenaventura, *HTR RPV Materials Damage Mechanisms*, Empesarios Agrupados Internacional Document No. 092-089-E-M-00003, Issue 1, 21 January 2002, HTR-M 02/02 D 1.4.27

[5] A Buenaventura, *HTR RPV Sensitive Zones*, Empesarios Agrupados Internacional Document No. 092-089-E-M-00004, Issue 1, 25 January 2002, HTR-M 02/02 D 1.4.28

[6] M T Cabrillat and A Buenaventura, *HTR-M WP 1.5: Design Rule Check*, CEA Document NT-SERI-LCSI-02/4017, Indice 0, 7 April 2002, HTR-M 02/08 D 1.1.40

[7] C Escaravage, *Identification and code status of pressure vessel candidate materials*, Framatome ANP Document EVED DC 02 0065 ECG/CPA Rev A, February 2002, HTR-M 02/04 D 1.1.31

[8] C Escaravage, *Compared Properties of Pressure Vessel Candidate Materials*, Framatome ANP Document EVED DC 02 0357 ECG/CPA., Rev A, 22/08/02, HTR-M-02/09/1.1.41

[9] A. A. Braithwiate, *Review of irradiation and thermal ageing effects in modified 9Cr 1Mo steel*, NNC Report C6463/TR/0zz, November 2002, HTR-M-02/1-D-1.1.48

[10] M. T. Cabrillat, *Effect of environment on the material of GT-MHR vessel*, NT – SERI – LCSI – 03/4019, October 2003, HTR-M-03/05-D-1.1.70

[11] J.B.J. Hegeman, J.H. Rantala, *HTR Vessel Materials, Specification of the sample selection, irradiation and PIE of mod. 9Cr steel*, NRG report 20585/03.52037/P, January 2003, HTR-M-03/02-D-1.4.63

[12] J.B.J. Hegeman, *Loading report LYRA-08 (304-08), irradiation in the frame of HTR-m*, NRG Report 20585/03.56740/P, December 2003

[13] J. Rensman, F. Schmalz, R. d. Boef, F.P. v.d. Broek, J. Boskeljon, *NRG SPIRE contribution: Mechanical Test Results from MTR Irradiation up to 3 dpa at 250°C*, NRG Report 20564/04. 62317/P, October 2004

[14] D. Pierron, *Modified 9Cr-1Mo steel, manufacturing of welded joints*, Framatome ANP, TFCW 03.3566, July 2004

[15] ECCC Recommendations 1999, Creep Data Validation and Assessment Procedures, European Creep Collaborative Committee (ECCC) 1999

[16] R. D. W. Bestwick, *Proposed creep rupture test conditions for the HTR-M irradiation experiment on a modified 9Cr-1Mo steel weld*, HTR-M 03/08-D-1 4 78, August 2003

[17] D. Buckthorpe, *Minutes of the 3rd HTR-M plus M1 Progress Meeting*, HTR-M-02/5-M-0-0-33, April 2002

[18] B. Acosta, LYRA, *HFR Irradiation Faci**L**it**Y** for the Eu**R**opean Network **A**MES (Ageing Materials European Strategy),* Design and Safety Report, Technical Memorandum HFR/02/4701, Petten, June 2002

[19] B. Acosta, *LYRA - 08 Experiment for "HTR-M" irradiation Exp. 304-08, experiment summary, JRC NSU/CA/BA/040302.01*, Petten, March 2004

[20] W. Freudenreich, J. Hegeman, *HTR-M – Activation analysis – (up to 500 days after irradiation) of the Vessel steel Modified 9Cr 1 Mo for the LYRA irradiation*, HTR-M-04/05-D-1.4.88, Petten, May 2004

[21] W.R. Corwin, A.M. Hougland, *Effect of specimen size and material condition on the charpy impact properties of 9Cr-1Mo-V-Nb steel*, in: The use of small-scale specimens for testing irradiated materials, ASTM STP 888, ed. W.R. Corwin, G.E. Lucas, 1986, 325-338

[22] F.Abe, H. Kayano, *Effect of specimen size on ductile to brittle transition behavior of martensitic 9Cr after various heat treatements*, Journal of Nuclear Materials 232, 1996, 44-51

appendix A Material specification

The data below is obtained from the report by FRAMATOME ANP [14].

Base Material

The coupons were taken from a 150mm thick plate manufactured by MARREL (INDUSTEEL)
Heat Number 88295 - plate Number 88295-1
The following heat treatments were performed :

- Austenitization 1070°C, then water quenching.
- Tempering 765°C-6h45

The acceptance tests of the plate were carried out on a few specimens after Austenitization + tempering and after the following Stress Relieving heat treatment 750°C-15h.

Filler metal

KOBE wire – product name TGS-9CB – diameter of wire 12mm.
Lot EZ00773.

WELDING

Both welded joints are performed in the same conditions. MC/TS 1973 Seam is intended for welding test and mechanical characterization TFCW 2056 seam is the contractual seam.

Welding is as follows:

- Preheating: 150-225°C
- Interpass temperature: 190-210°C
- Post heating : 300-350°C for a minimum of 2 hours
- 2 passes by layer

Heat treatment
The PWHT applied is given below:

- Heating rate : ≤ 25°C / h (from 300°C)
- Holding time : 760±5°C – 10 h 30
- Cooling rate : ≤ 25°C / h (down to 300°C)

CREUSOT-LOIRE INDUSTRIE Division CREUSOT-MARREL Usine de CHATEAUNEUF	CLIENT Customer - Kunde: FRAMATOME ST MARCEL CDE CLIENT Customer order - Auftrag n: 89.03182702.P.70012 PROJET Project - Projekt: CDE CREUSOT-MARREL Creusot-Marrel order: 25 771.L.	**ANALYSES CHIMIQUES** Chemical Analysis Chemische Analyse

NUANCE steel grade - Werkstoff: Z 10 CDV - Nb 9.1

SPECIFICATION specification spezifikation: MC / TS 88.2154 rev.0 + cde client

TRAITEMENT THERMIQUE SUR TOLE: TREMPE + REVENU
Heat treatment on plate - Wärmebehandlung Zustand am blech

COULEE N° Heat n° - Schmelze nr: 88 295 | TOLE N° Plate n° - Blech nr: 88 295.1 | REPERE Item:

DIMENSIONS sizes - Abmessungen: 1 tôle 2270 x 3000 x 150 mm

%	ANALYSE COULEE Heat analysis-Schmelze analyse		ANALYSE PRODUIT Product analysis-Stückanalyse		
	IMPOSE Required Soll	OBTENU Obtained Ist	IMPOSE Required Soll	OBTENU HAUT Obtained top Ist kopf - ½ EP	OBTENU BAS Obtained btm Ist fuss
C	0.080 / 0.120	0.105	0.080 / 0.120	0.110	
Mn	0.30 / 0.50	0.440	0.30 / 0.50	0.450	
Si	0.20 / 0.50	0.240	0.20 / 0.50	0.250	
Ni	≦ 0.20	0.080	≦ 0.20	0.085	
Cr	8.00 / 9.00	8.410	8.00 / 9.00	8.410	
Mo	0.85 / 1.05	0.950	0.85 / 1.05	0.960	
Cu	≦ 0.10	0.035	≦ 0.10	0.030	
Al	≦ 0.040	0.013	≦ 0.040	0.013	
S	≦ 0.010	0.0016	≦ 0.010	0.0014	
P	≦ 0.020	0.008	≦ 0.020	0.008	
Sn	INFO	0.004	INFO	0.004	
V	0.18 / 0.25	0.250	0.18 / 0.25	0.250	
Nb	0.06 / 0.10	0.080	0.06 / 0.10	0.085	
N_2	0.030 / 0.070	0.033	0.030 / 0.070	0.034	
As	INFO	0.008	INFO	0.008	

date et résultats du contrôle Date and results of examination-Prüfdatum : 6.10.89

[X] conformes à la spécification imposée
conforming to required specification
Anforderungen gemäss spezifikation

[ ] non conformes-voir FA n° du
not conforming-see NCR n° dated
Unzulässige befunde-siehe QAB vom

RESULTATS VERIFIES Results checked Ergebnisse geprüft am	CREUSOT-MARREL	FRAMATOME		
24 OCT. 1989	CREUSOT LOIRE INDUSTRIE Division CREUSOT-MARREL [illegible] A. MILLET			

CREUSOT-LOIRE INDUSTRIE *Division CREUSOT-MARREL Usine de CHATEAUNEUF* <R>	*ANALYSES CHIMIQUES* *Chemical Analysis Chemische Analyse*

CLIENT Customer - Kunde: FRAMATOME ST MARCEL

CDE CLIENT Customer order - Auftrag n: 89.03182702.P.70012

PROJET Project - Projekt:

CDE CREUSOT-MARREL Creusot-Marrel order: 25 771.L.

NUANCE steel grade - Werkstoff: Z 10 CDV - Nb 9.1

SPECIFICATION specification spezifikation: MC / TS 88.2154 rev.0 + cde client

TRAITEMENT THERMIQUE SUR TOLE Heat treatment on plate - Wärmebehandlung Zustand am blech: TREMPE + REVENU

COULEE N° Heat n° - Schmelze nr: 88 295 — TOLE N° Plate n° - Blech nr: 88 295.1 — REPERE Item:

DIMENSIONS sizes - Abmessungen: 1 tôle 2270 x 3000 x 150 mm

%	ANALYSE COULEE Heat analysis-Schmelze analyse: IMPOSE Required Soll	OBTENU Obtained Ist	ANALYSE PRODUIT Product analysis-Stückanalyse: IMPOSE Required Soll	OBTENU HAUT Obtained top Ist kopf - ½ EP	OBTENU BAS Obtained btm Ist fuss
Sb	INFO	0.0011	INFO	0·011	
Ti	INFO	< 0.005	INFO	0·004	
B	INFO	0.0009	INFO	0·0008	
W	INFO	< 0·020	INFO	< 0·020	
O_2	INFO	10 ppm	INFO		
Zr	INFO	< 0·005	INFO	< 0,005	

date et résultats du contrôle Date and results of examination-Prüfdatum : 6.10.89

[X] conformes à la spécification imposée / conforming to required specification / Anforderungen gemäss spezifikation

[ ] non conformes-voir FA n° du / not conforming-see NCR n° dated / Unzulässige befunde-siehe QAB vom

RESULTATS VERIFIES Results checked Ergebnisse geprüft am	CREUSOT-MARREL	FRAMATOME		
24 OCT. 1989	CREUSOT LOIRE INDUSTRIE Division CREUSOT MARREL [signature] A. MILLET			

appendix B Irradiation history

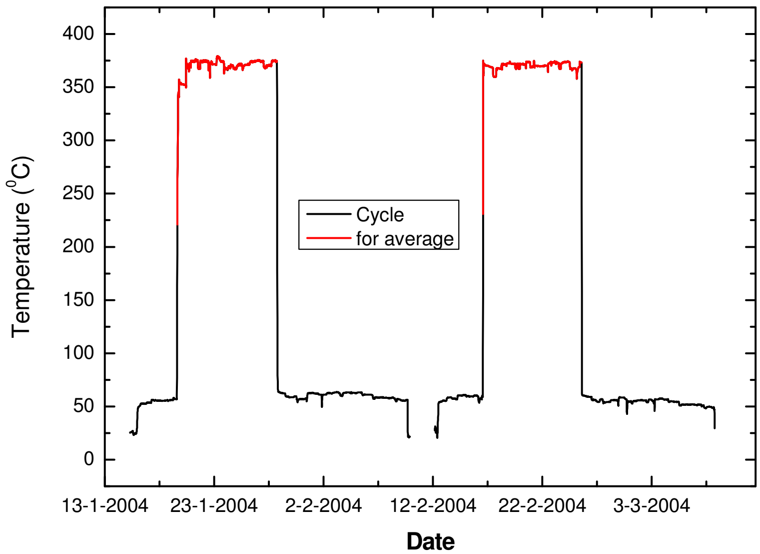

figure 31   Average irradiation temperature of the LYRA during the two irradiation cycles

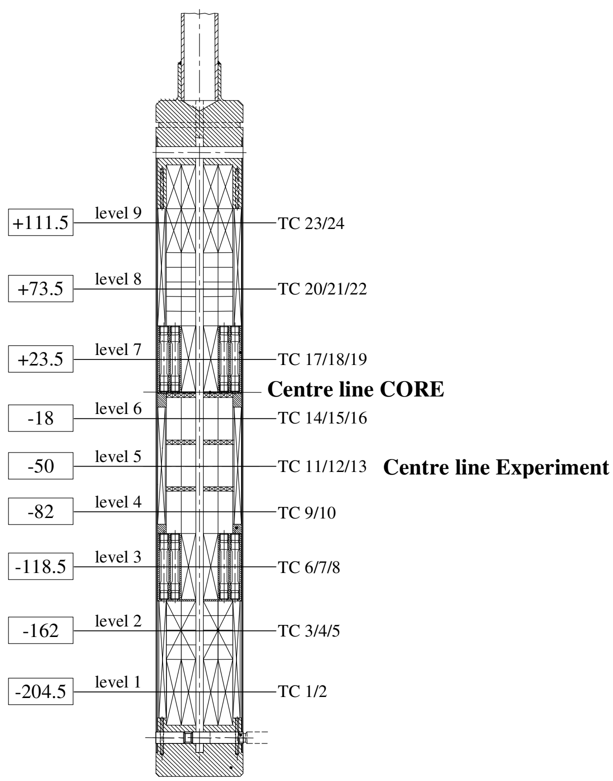

figure 32   Vertical distribution of the thermocouples with respect to the centreline of the HFR core

appendix C Test results

table 8 tensile results for mod. 9Cr materials, base metal

Material	Specimen number	Neutron dose 10^{24} (E>0.1MeV)	Neutron dose 10^{24} (E>1MeV)	Damage (dpa)	Temperature (°C)	YS $\sigma_{0.2\%}$ (MPa)	$\sigma_{0.5\%}$ (MPa)	$\sigma_{1.0\%}$ (MPa)	$\sigma_{2.0\%}$ (MPa)	$\sigma_{5.0\%}$ (MPa)	$\sigma_{10\%}$ (MPa)	$\Delta\sigma_{0.2\%}$ (MPa)	UTS (MPa)	Total elong. (record.) (%)	Fract elong. (meas.) (%)	Uniform elong. (%)	Red. of area (%)
Base metal	L209				20	465	480	493	550	610	633		634	27.3		10.9	
L	L280				20	467	477	505	550	611	633		634	26.2		10.7	
NRG	L205				550	338	348	356	359	353	337		360	28.7		2.1	
NRG	L222				550	324	336	342	345	335	321		345	31.9		1.9	
Base metal Irradiated *L*	L208	10.4	4.2	6.4	27	506	508	519	550	613	646	40	649	26.6	26.6	10.7	77.5
	L281	9.6	3.9	5.9	27	505	507	520	549	614	646		647	27	27	9.8	75.9
	L229	9.0	3.6	5.5	375	417	432	448	478	514	502		519	19.6	19.6	6.7	68.9
	L290	9.0	3.7	5.6	375	410	422	443	469	506	490		513	19.4	19.4	7.2	81
	L226	8.8	3.6	5.4	450	375	395	418	443	468	457		471	22.2		6.1	
	L289	9.3	3.8	5.7	450	384	402	421	448	475	454		476	20.5	20.5	5.8	80.3
	L211	10.1	4.1	6.3	550	326	347	359	364	357	335	4	365	25.4	25.4	2.2	88.6
	L282	9.8	4.0	6.0	550	328	343	352	356	350	334		357	29.9	29.9	2.3	91.5
Base metal	L182				20	460	470	487	540	599	630		631	28.7		10.7	
T	L265				20	453	467	480	538	597	625		625	27.4		11.3	
Base metal Irradiated *T*	L183	11.4	4.7	7.1	27	505	505	517	545	611	644	42	646	27.4	27.4	11.2	77.6
	L264	9.1	3.7	5.6	27	491	496	506	539	604	639		641	27.6	27.6	10.8	72.4
	L192	8.8	3.6	5.4	375	408	422	441	471	509	500		515	19.7	19.7	7	70.1
	L275	9.5	3.9	5.9	375	408	418	439	465	504	494		510	19.6	19.6	7.1	77.5
	L191	8.6	3.5	5.4	450	378	396	415	444	475	454		478	19.4		5.4	
	L272	9.9	4.1	6.1	450	372	391	413	442	474	463		477	21.3	21.3	6.7	78.3
	L184	11.0	4.5	6.8	550	311	332	343	348	342	325		349	34.4		2.3	
	L267	9.2	3.7	5.7	550	311	328	339	345	340	322		345	27.8	27.8	2.6	92.1

table 9 tensile results for mod. 9Cr materials, weld metal and cross-weld

Material	Specimen number	Neutron dose 10^{24} (E>0.1MeV)	Neutron dose 10^{24} (E>1MeV)	Damage (dpa)	Temperature (°C)	YS $\sigma_{0.2\%}$ (MPa)	$\sigma_{0.5\%}$ (MPa)	$\sigma_{1.0\%}$ (MPa)	$\sigma_{2.0\%}$ (MPa)	$\sigma_{5.0\%}$ (MPa)	$\sigma_{10\%}$ (MPa)	$\Delta\sigma_{0.2\%}$ (MPa)	UTS (MPa)	Total elong. (record.) (%)	Fract elong. (meas.) (%)	Uniform elong. (%)	Red. of area (%)
Weldmetal	L135				20	504	494	502	518	597	631		635	32.4		13.4	
	L164				20	494	497	498	520	595	631		635	31.2		12.9	
Weldmetal Irradiated	L134	11.0	4.5	6.8	27	418	467	530	551	593	631	nd*	654	37.7		15.4	
	L165	10.1	4.2	6.3	27	515	511	513	534	598	633	16	638	31.9		12.5	
	L246	9.2	3.8	5.7	375	413	417	433	458	496	506		513	21.9	21.9	6.9	84.9
	L241	9.6	3.9	5.9	375	427	429	443	470	506	517		519	22.5	22.5	8.8	80.8
	L163	10.4	4.3	6.5	450	360	376	391	417	445	446		451	23.6	23.6	7.2	84.1
	L238	9.4	3.8	5.8	450	383	398	414	437	458	455		461	25.1	25.1	6.2	84.5
	L161	10.7	4.4	6.6	550	282	303	316	322	323	314		326	33.6		3.9	
	L167	8.3	3.4	5.1	550	271	299	311	322	321	311		324	39.1		2.8	
Crossweld	K847				20	450	467	490	529	591	622		622	22.7		10.0	
	L177				20	458	475	491	522	593	624		625	22.9		10.4	
Crossweld Irradiated	K848	10.8	4.4	6.7	27	488	506	533	542	603	636	36	637	22.2	22.2	9.9	75.5
	L176	9.3	3.8	5.7	27	492	510	517	544	606	637		638	22.1		10.3	
	K854	9.7	4.0	6.0	375	398	418	439	467	496	438		498	15.7	15.7	4.5	83.5
	L180	9.5	3.9	5.9	375	391	409	428	455	492	465		501	16.7	16.6	6.1	82.2
	K850	10.4	4.3	6.5	450	367	387	404	430	458	443		462	20.8	20.8	6.3	81.3
	L251	9.7	4.0	6.0	450	371	393	416	441	460	409		462	16.7		4.6	
	K852	10.1	4.1	6.2	550	309	324	334	339	332	306		339	22.2	22.2	2.3	88.1
	L248	9.6	3.9	5.9	550	319	334	345	351	342	297		352	19.8	19.8	2.3	89.2

* not determined due to large deviation; therefore this test is excluded.

table 10 550°C Creep results for mod. 9Cr materials, Base metal, weld metal and cross-weld

Material	Specimen number	Neutron dose 10^{24} (E>0.1MeV)	Neutron dose 10^{24} (E>1MeV)	Damage (dpa)	Creep Stress (MPa)	Rupture time (hrs)	Minimum creep rate (%/hrs)	Time to ε=0.5% (hrs)	Time to ε=1.0% (hrs)	Time to ε=2.0% (hrs)	Time to ε=5.0% (hrs)	Fracture elongation (%)	Reduction of area 9%)
Base metal L	L213				232	86.3	$5.81\cdot10^{-2}$	1.8	8.1	24.9	59.6	33.6	89.3
	L232				205	420.2	$1.28\cdot10^{-2}$	5.0	26.8	99.9	288.5	33.6	89.3
	L284				190	1061.2	$4.85\cdot10^{-3}$	8.6	54.7	234.0	736.5	30.8	90.4
	L296				172	6511	$6.34\cdot10^{-4}$	32.7	259.7	1444.0	5067.1	25.4	88.3
Base metal L Irradiated	L212	9.4	3.8	5.8	226.4	98.3	$4.98\cdot10^{-2}$	2.3	9.3	28.3	72.3	15.2	
	L233	9.9	4.0	6.1	208.6	317.3	$1.61\cdot10^{-2}$	4.1	19.2	77.3	229.3	26.0	
	L285	10.0	4.0	6.2	190.8	1309.5	$3.80\cdot10^{-3}$	6.8	50.3	247.3	944.0	16.5	
	L295	8.5	3.5	5.2			Running*						
Base metal T	L186				232	59.7	$8.42\cdot10^{-2}$	1.1	5.3	16.6	41.2	34.4	90.1
	L197				205	284.9	$1.75\cdot10^{-2}$	2.8	18.2	71.2	198.2	34.5	91.6
	L269				185	1205.2	$4.19\cdot10^{-3}$	10.3	66.1	277.9	845.8	33.9	89.7
	L278				170	4999.9	$8.34\cdot10^{-4}$	27.5	217.9	1122.7	3872.0	28.8	86.7
Base metal T Irradiated	L187	9.4	3.8	5.8	224.1	86.3	$5.57\cdot10^{-2}$	1.3	6.7	23.7	64.3	11.9	
	L196	9.9	4.0	6.1	206.3	352.6	$1.42\cdot10^{-2}$	3.4	18.4	77.6	261.6	10.4	
	L268	10.0	4.0	6.2	186.8	1444.1	$3.16\cdot10^{-3}$	8.3	59.3	307.3	1126.0	13.6	
	L279	8.5	3.5	5.2			Running*						
Weldmetal	L162				232	23.1	$3.18\cdot10^{-1}$	0.5	1.9	5.0	12.3	51.0	92.0
	L235				190	463.6	$1.40\cdot10^{-2}$	3.1	15.6	65.8	265.1	29.3	84.2
	L244				182	920.6	$7.14\cdot10^{-3}$	6.0	32.3	135.2	523.4	25.5	90.2
	L170				175	3517.5	$1.33\cdot10^{-3}$	7.1	56.7	395.0	2375.7	26.8	84.0
Weldmetal Irradiated	L247	9.2	3.7	5.7	215.7	60.3	$1.26\cdot10^{-1}$	1.5	4.8	12.8	32.3	26.3	
	L234	9.3	3.8	5.8	191.4	524.6	$1.30\cdot10^{-2}$	3.1	16.1	70.3	292.5	20.4	
	L169	9.9	4.0	6.1	175.3	1820.0	$2.99\cdot10^{-3}$	8.3	40.3	223.3	1183.8	16.3	
		8.2	3.4	5.1			Running*						
Crossweld	L257				205	163.0	$2.77\cdot10^{-2}$	3.0	13.6	46.76	129.9	20.4	88.6
	L175				190	319.8	$1.14\cdot10^{-2}$	6.0	32.2	115.1	282.2	18.9	88.6
	L262				180	1172.7	$4.06\cdot10^{-3}$	10.1	71.5	305.2	899.1	20.8	84.8
	L253				170	2857.2	$8.74\cdot10^{-4}$	13.7	121.1	877.1	2494.3	20.0	90.3
Crossweld Irradiated	L256	9.1	3.7	5.6	212.8	165.4	$3.06\cdot10^{-2}$	4.1	16.3	46.4	128.4	11.3	
	L174	9.0	3.7	5.5	190.4	430.0	$9.38\cdot10^{-3}$	10.3	45.3	152.2	377.0	11.0	
	L263	9.5	3.9	5.9	185.6	1367.1	$3.01\cdot10^{-3}$	12.8	71.1	341.6	1154.6	12.73	
	L252	8.5	3.4	5.2	179.1	2366.4	$1.38\cdot10^{-3}$	20.5	113.3	612.7	2170.4	10.3	

* tests are still being performed at the time of publication

table 11 Results of the (sub-size) impact tests of the 9 Cr martensitic welded joint

Material	Specimen number	Temperature (°C)	Impact energy A_v (J)	Lateral expansion (mm)	Broken	Specimen number	Neutron dose 10^{24} (E>0.1MeV)	Neutron dose 10^{24} (E>1MeV)	Damage (dpa)	Temperature (°C)	Impact energy A_v (J)	Lateral expansion (mm)	Broken
	Reference					**Irradiated**							
Base metal T-L	K942	-150	0.5	0.05	Y	K961	9.9	4.1	6.1	-150	0.6	0.02	Y
	K938	-110	0.4	0.1	Y	K960	9.8	4.0	6.1	-100	0.6	0.02	Y
	K954	-110	1.05	0.15	Y	K948	9.6	3.9	5.9	-100	1.3	0.04	Y
	K947	-100	0.9	0.1	Y	K956	9.5	3.9	5.9	-75	6	0.6	N
	K958	-100	0.34	0.05	Y	K957	9.7	3.9	6.0	-75	7.5	0.66	N
	K943	-90	5.8	0.65	N	K940	9.7	4.0	6.0	-50	7	0.69	N
	K951	-85	5.9	0.75	N	K937	9.7	4.0	6.0	-50	11	0.79	N
	K959	-85	6.5	0.75	N	K944	9.3	3.8	5.8	-25	10	0.74	N
	K939	-50	9	1	N	K941	9.6	4.0	6.0	-25	10.8	0.79	N
	K950	-15	8.6	1	N	K949	9.7	4.0	6.0	-15	11.3	0.82	N
	K935	0	8.95	1	N	K952	9.9	4.0	6.1	-15	10	0.83	N
	K946	125	8.9	1.05	N	K953	9.4	3.8	5.8	0	10.2	0.86	N
	K955	250	7.95	1.1	N	K936	9.7	4.0	6.0	0	12.5	0.89	N
	K934	375	7.6	1	N	K945	9.4	3.8	5.8	50	11.5	0.84	N
	K962	375	8.15	1	N	K933	9.8	4.0	6.1	375	9.4	0.96	N
Base metal L-T	K973	-150	0.3	0.05	Y	K983	10.2	4.2	6.3	-150	0.6	0	Y
	K968	-110	0.6	0.1	Y	K967	9.9	4.0	6.1	-125	0.6	0	Y
	K984	-110	0.5	0.1	Y	K978	10.4	4.3	6.5	-100	0.8	0.02	Y
	K988	-100	0.75	0.1	Y	K986	10.4	4.2	6.4	-100	1.4	0.05	Y
	K977	-100	3.2	0.35	Y	K982	10.7	4.4	6.7	-85	10.5	0.88	N
	K981	-85	5.5	0.65	N	K991	10.8	4.4	6.8	-85	1.8	0.11	N
	K989	-85	6.05	0.7	N	K970	9.9	4.0	6.1	-50	10	0.96	N
	K969	-50	7.4	0.85	N	K987	10.5	4.3	6.5	-50	9.8	0.73	N
	K980	-15	8.7	1	N	K990	10.7	4.4	6.6	-25	10.5	0.86	N
	K965	0	9.1	1	N	K979	10.6	4.3	6.5	-15	11.3	0.92	N
	K976	125	8.65	1.05	N	K974	10.2	4.1	6.3	0	11.2	0.94	N
	K985	250	8.2	1.1	N	K966	10.0	4.1	6.2	0	12.8	0.81	N
	K964	375	8.15	1.08	N	K971	9.9	4.0	6.1	50	11.6	0.87	N
	K992	375	8.6	1	N	K975	10.3	4.2	6.4	125	10	0.96	N
						K963	10.0	4.1	6.2	375	9.5	0.98	N

table 12 Results of the (sub-size) impact tests of the heat affected zone of the 9 Cr martensitic welded joint

Material	Specimen number	Temperature (°C)	Impact energy A_v (J)	Lateral expansion (mm)	Broken	Specimen number	Neutron dose 10^{24} (E>0.1MeV)	Neutron dose 10^{24} (E>1MeV)	Damage (dpa)	Temperature (°C)	Impact energy A_v (J)	Lateral expansion (mm)	Broken
	Reference					**Irradiated**							
Heat Affected Zone (HAZ)	L371	-150	0.4	0	Y	L345	9.8	4.0	6.1	-151	0.8	0.02	Y
	L331	-150	0.5	0	Y	L332	9.7	4.0	6.0	-150	0.7	0.02	Y
	L350	-140	0.73	0.04	Y	L344	10.6	4.3	6.5	-125	1.3	0.02	Y
	L398	-140	0.62	0.02	Y	L352	10.7	4.4	6.6	-125	2.5	0.11	Y
	L386	-130	0.58	0.02	Y	L349	8.4	3.4	5.2	-110	3.3	0.25	N
	L362	-130	1.5	0.09	Y	L340	9.7	4.0	6.0	-110	5	0.42	N
	L366	-120	5.2	0.51	Y	L353	9.8	4.0	6.0	-100	2.2	0.17	N
	L354	-120	1.6	0.11	Y	L356	9.6	4.0	6.0	-100	6.2	0.56	N
	L394	-120	3.65	0.35	Y	L360	10.9	4.4	6.8	-85	11.3	0.85	N
	L339	-110	4.3	0.46	Y	L341	8.5	3.4	5.2	-85	12.6	0.89	N
	L379	-110	3.2	0.34	Y	L368	8.0	3.3	5.0	-85	8.7	0.64	N
	L390	-95	7.3	0.7	N	L365	8.4	3.4	5.2	-75	12.4	0.95	N
	L346	-95	5.64	0.6	N	L361	9.7	4.0	6.0	-75	8.5	0.72	N
	L382	-95	5.5	0.54	Y	L372	8.3	3.4	5.1	-63	11.6	0.82	N
	L399	-85	6.6	0.75	N	L369	8.2	3.3	5.1	-63	7.9	0.77	N
	L359	-85	5	0.57	Y	L336	10.4	4.3	6.5	-50	10.2	0.89	N
	L358	-70	8.8	0.89	N	L337	9.9	4.0	6.1	-50	11	0.79	N
	L338	-70	8.9	0.86	N	L373	8.4	3.4	5.2	-25	10	0.85	N
	L378	-60	8.9	0.93	N	L376	8.5	3.5	5.3	-25	11.9	0.77	N
	L406	-60	7.5	0.83	N	L329	9.9	4.0	6.1	0	10	0.84	N
	L335	-50	9	0.93	N	L333	8.5	3.4	5.2	0	11.5	0.84	N
	L375	-50	9.25	0.94	N	L364	9.6	4.0	5.9	25	10.8	0.83	N
	L342	-35	9.18	0.95	N	L357	8.4	3.4	5.2	25	11	0.84	N
	L370	-35	9.1	0.94	N	L348	9.7	4.0	6.0	175	10.5	0.86	N
	L351	-15	9.1	0.98	N	L328	10.3	4.2	6.4	375	9.8	0.97	N
	L391	-15	10.2	0.98	N								
	L330	0	9.2	0.95	N								
	L402	0	9.06	0.99	N								
	L383	20	9	1.02	N								
	L343	20	9	0.98	N								
	L334	50	9.2	0.95	N								
	L374	50	9.6	0.9	N								
	L355	125	8.8	1.02	N								
	L395	125	8.7	1.06	N								
	L347	250	8.2	1.06	N								
	L387	250	8.8	1.08	N								
	L403	375	8.5	1.02	N								
	L367	375	9.1	1.04	N								
	L363	375	9.2	1.03	N								
	L327	375	7.7	1.1	N								

table 13 Results of the (sub-size) impact tests of the weld metal of the 9 Cr martensitic welded joint

Material	Specimen number	Temperature (°C)	Impact energy A_v (J)	Lateral expansion (mm)	Broken	Specimen number	Neutron dose 10^{24} (E>0.1MeV)	Neutron dose 10^{24} (E>1MeV)	Damage (dpa)	Temperature (°C)	Impact energy A_v (J)	Lateral expansion (mm)	Broken
	Reference					Irradiated							
	L108	-150	0.49	0.05	Y	L109	9.6	3.9	5.9	-150	0.8	0.02	Y
	L103	-150	0.5	0.05	Y	L118	9.9	4.0	6.1	-125	4.6	0.3	Y
	L112	-140	1.25	0.1	Y	L122	9.8	4.0	6.1	-125	1.3	0.04	Y
	L119	-130	0.55	0.05	Y	L114	10.0	4.0	6.2	-110	0.9	0.03	Y
	L104	-120	7.9	0.8	N	L117	10.0	4.0	6.1	-110	11.4	0.91	N
	L115	-110	10.4	1	N	L105	9.6	3.9	6.0	-98	9.2	0.82	N
	L099	-110	7.85	0.8	N	L113	9.5	3.9	5.9	-98	12.0	0.95	N
Weldmetal	L120	-85	9.4	1	N	L121	9.9	4.0	6.1	-85	12.5	1	N
	L100	-50	10.5	1.1	N	L102	10.0	4.1	6.2	-85	10.2	0.87	N
	L111	-15	10.1	1	N	L101	9.8	4.0	6.1	-50	13.1	0.98	N
	L096	0	10.1	1.1	N	L106	9.6	3.9	6.0	-50	12.0	0.91	N
	L107	125	9.75	1.15	N	L110	9.5	3.9	5.9	0	12.4	1	N
	L116	250	8.65	1.1	N	L097	9.6	3.9	5.9	0	12.1	0.93	N
	L095	375	8.95	1.05	N	L098	9.7	4.0	6.0	375	10.9	0.93	N
	L123	375	8.3	1.05	N								

table 14 Results of the full-size charpy specimens (Reference)

Material	Specimen number	Temperature (°C)	Impact energy A_v (J)	Lateral expansion (mm)	Broken	Material	Specimen number	Temperature (°C)	Impact energy A_v (J)	Lateral expansion (mm)	Broken
	Reference						Reference				
	K897	-150	3.8	0.05	Y		L139	-150	6.2	0.08	Y
	K879	-110	6.5	0.1	Y		L151	-110	16	0.26	Y
	K893	-90	14.5	0.21	Y		L143	-90	27	0.28	Y
	K883	-70	51	0.66	Y		L149	-80	84	1.13	Y
	K891	-50	58	0.83	Y		L145	-75	204	2.36	Y
Base metal T-L	K877	-35	130	1.81	N	Weldmetal T-L	L157	-70	195	2.31	N
	K889	-20	153.	2.23	Y		L147	-50	227.3	2.57	N
	K885	0	160	2.15	N		L153	-20	290	2.37	N
	K887	20	220	2.49	N		L155	20	291.5	2.72	N
	K895	125	228	2.48	N		L141	375	300		N
	K881	250	271	1.61	Y						
	K899	375	300		N						
HAZ	K902	20	226	2.47	N						

table 15 J-R fracture toughness test results for the mod. 9Cr welded joint valid for CT specimens with B = 10 mm and W = 22.5 mm

Material	Specimen number	Neutron dose 10^{24} (E>0.1MeV)	Neutron dose 10^{24} (E>1MeV)	Damage (dpa)	Testing temperature (°C)	a_0/W	Blunting Slope ESIS P2-90 (MPa)	J at end of test (kJ/m^2)	Δa at end of test (mm)	J at Δa=0.2mm (kJ/m^2)	$J_{0.2BL}$ (kJ/m^2)	$Δa_{0.2BL}$ (mm)	$J_{Q\ ASTM}$ (kJ/m^2)	$Δa_{Q\ ASTM}$ (kJ/m^2)	Max Force P_{max} during test (kN)	J at P_{max} (kJ/m^2)	Δa at P_{max} (mm)	Power law Constant	Power Law Exponent	$Δa_{Min}$ for Power law fit (mm)
Base metal L-T Irradiated	K838	9.8	4.0	6.1	24	0.59	2433	733	0.71	416	546	0.43			9.3	576	0.47	782	0.40	0.21
	K842	10.7	4.4	6.7	24	0.60	2433	1008	1.35	424	534	0.42	719	0.83	9.1	585	0.51	785	0.42	0.22
	K840	9.8	4.0	6.1	375	0.59	1926	437	0.65	250	306	0.36	414	0.65	7.4	340	0.43	491	0.43	0.20
	K844	9.7	4.0	6.0	375	0.60	1926	629	1.21	247	298	0.36	411	0.65	7.3	318	0.41	519	0.51	0.21
	K846	9.6	3.9	5.9	375	0.60	1926	528	0.90	249	318	0.37	422	0.65	7.4	310	0.34	513	0.46	0.20
Base metal T-L Irradiated	K828	10.4	4.2	6.4	24	0.59	2493	627	0.59	372	488	0.41			9.2	488	0.41	751	0.45	0.22
	K832	9.5	3.9	5.9	24	0.60	2493	1027	1.29	378	503	0.40	715	0.83	9.2	496	0.38	798	0.48	0.21
	K830	9.7	4.0	6.0	375	0.59	1977	403	0.61	228	287	0.35			7.5	283	0.34	484	0.48	0.21
	K834	10.0	4.1	6.2	375	0.59	1977	632	1.35	239	306	0.36	418	0.66	7.8	296	0.34	500	0.47	0.21
	K836	9.6	3.9	5.9	375	0.59	1977	484	1.24	216	251	0.34	298	0.53	7.1	210	0.17	394	0.40	0.20
Weldmetal Irradiated	L124	9.5	3.9	5.9	24	0.59	2380	1093	0.79	447	833	0.55			10	828	0.53	1174	0.55	0.20
	L128	10.4	4.2	6.4	24	0.59	2380	1632	1.37	464	799	0.54			9.7	792	0.52	1188	0.59	0.20
	L126	9.9	4.0	6.1	375	0.59	1953	654	0.82	323	435	0.43			7.6	488	0.53	657	0.46	0.20
	L130	9.7	4.0	6.0	375	0.59	1953	1048	1.55	317	412	0.42	629	0.87	7.6	450	0.48	701	0.57	0.21
	L132	9.3	3.8	5.7	375	0.59	1953	830	1.21	350	468	0.44	658	0.91	7.7	466	0.43	689	0.46	0.21
HAZ Irradiated	K818	10.7	4.4	6.6	24	0.59	2456	925	0.75	471	712	0.50			9.7	661	0.42	973	0.43	0.20
	K822	9.9	4.0	6.1	24	0.59	2456	1247	1.47	488	640	0.47	947	1.05	9.4	658	0.49	927	0.45	0.20
	K820	9.6	4.0	6.0	375	0.60	1917	594	0.73	321	431	0.43			7.5	447	0.47	640	0.45	0.20
	K824	9.9	4.0	6.1	375	0.59	1917	823	1.54	286	345	0.38	503	0.76	7.5	407	0.53	582	0.52	0.21
	K826	9.7	3.9	6.0	375	0.59	1917	714	0.93	301	412	0.42			7.6	456	0.50	682	0.55	0.21
commercial T91	C801	10.12	4.1	6.3	24	0.59	2493	835	1.44	344	425	0.38	557	0.70	10.3	406	0.34	648	0.41	0.21
	C802	10.45	4.3	6.5	24	0.59	2493	551	0.69	339	406	0.38	500	0.64	10.2	386	0.33	592	0.37	0.21
	C803	9.4	3.9	5.8	375	0.59	1977	447	1.25	180	211	0.31	264	0.49	8.5	208	0.30	371	0.46	0.21
	C804	9.5	3.9	5.9	375	0.58	1977	302	0.69	183	207	0.31	240	0.46	8.5	181	0.20	329	0.39	0.21

appendix D Raw data curves

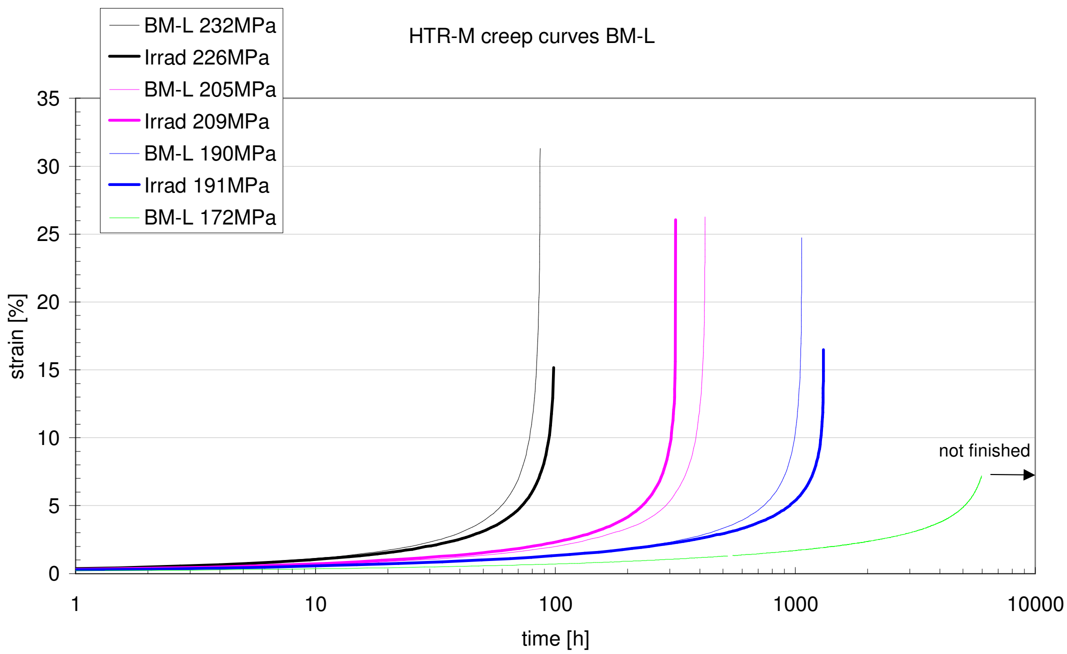

figure 33 Individual creep curves for the base material specimens in the longitudinal orientation.

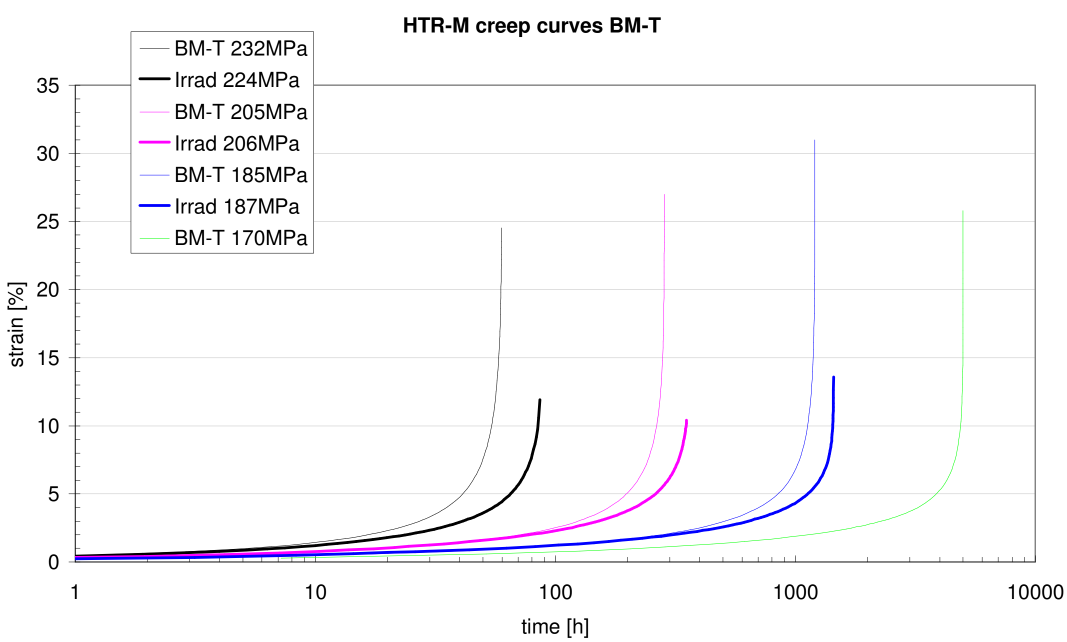

figure 34 Individual creep curves for the base material specimens in the transverse orientation.

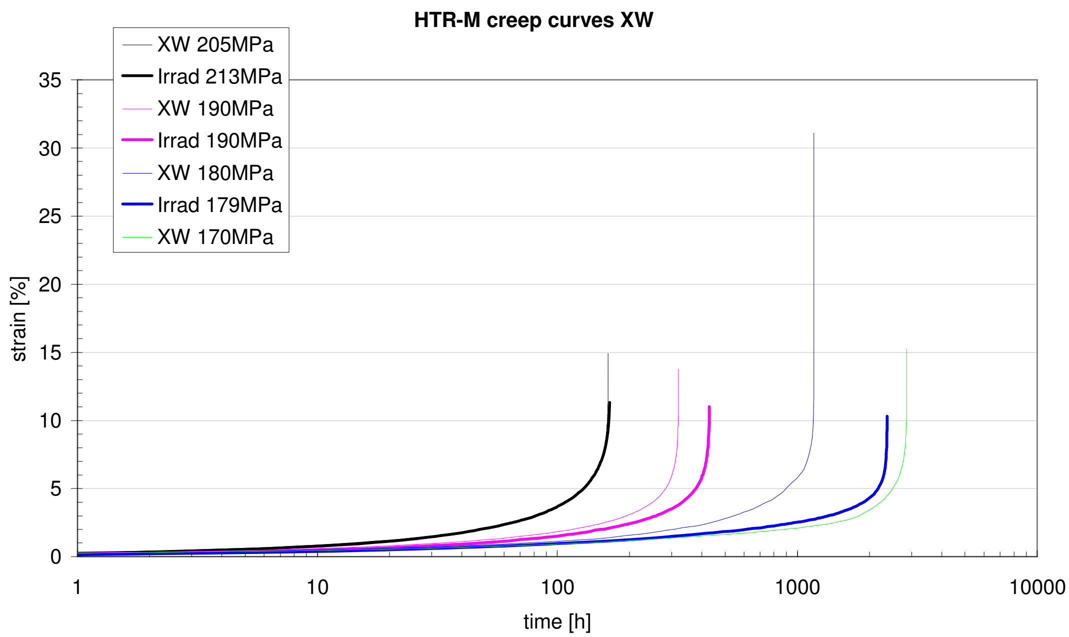

figure 35 Individual creep curves for the weld metal specimens.

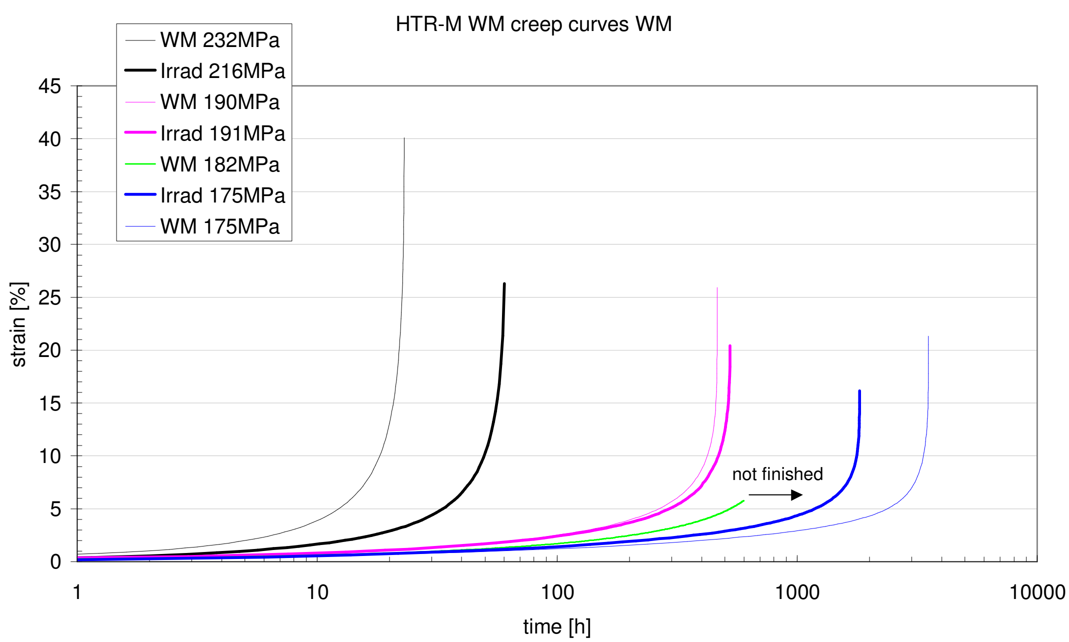

figure 36 Individual creep curves for the base material specimens in the transverse orientation

appendix E Failure locations of the unirradiated cross-weld tests

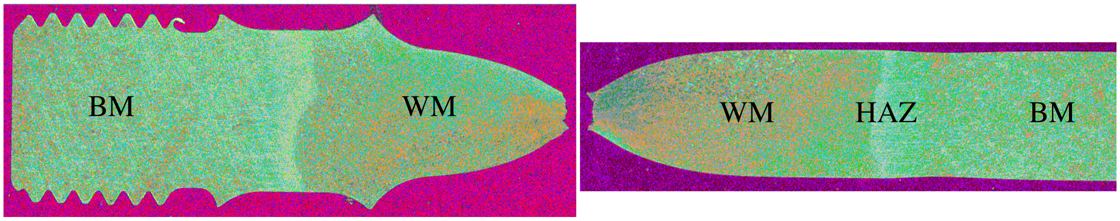

figure 37 Creep specimen L257, stress of 205MPa, rupture time 163.0h, Failure in weld metal. Note necking at the HAZ on the right

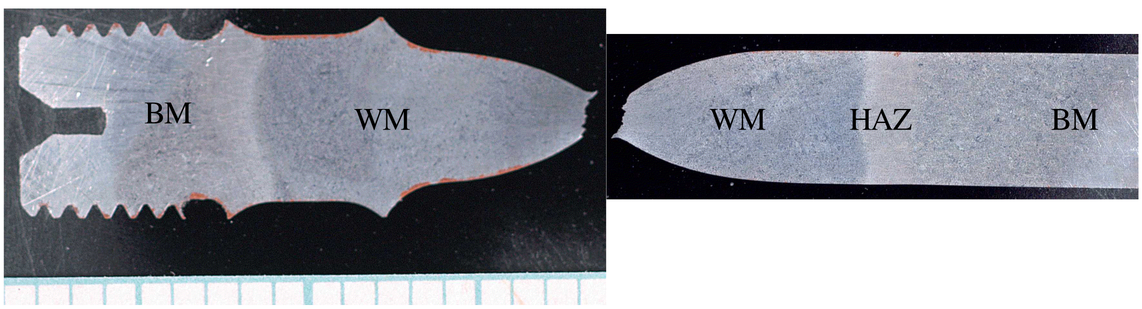

figure 38 Creep specimen L175, stress of 190MPa, rupture time 319.8h, Failure in weld metal. Note slight necking at the HAZ on the right. Millimeter-scale on the left. Shade changes on the threaded part caused by uneven polishing. The same applies to the BM on the far right

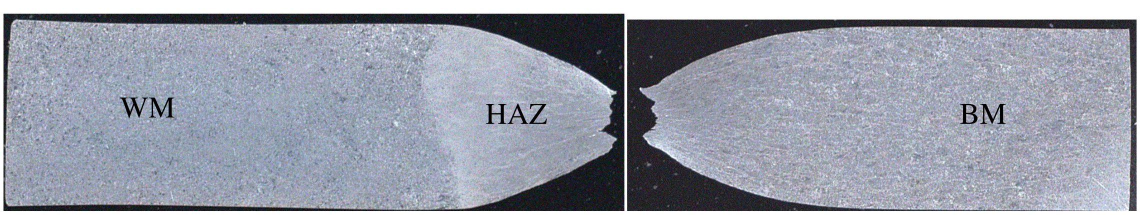

figure 39 Creep specimen L262, stress of 180MPa, rupture time 1173h, Failure in the intercritical of the HAZ in the BM.

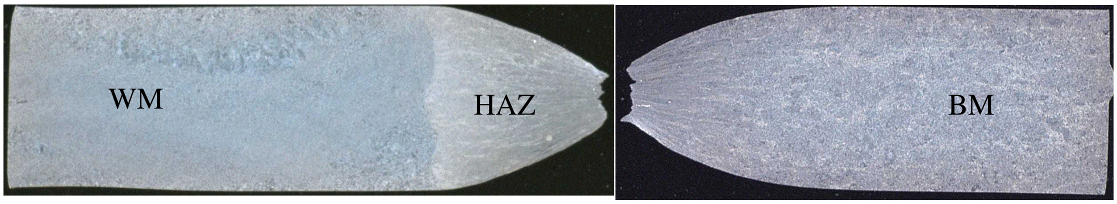

figure 40	Creep specimen L2532, stress of 170MPa, rupture time 2857h, Failure in the intercritical of the HAZ in the BM.

appendix F Final cutting schemes

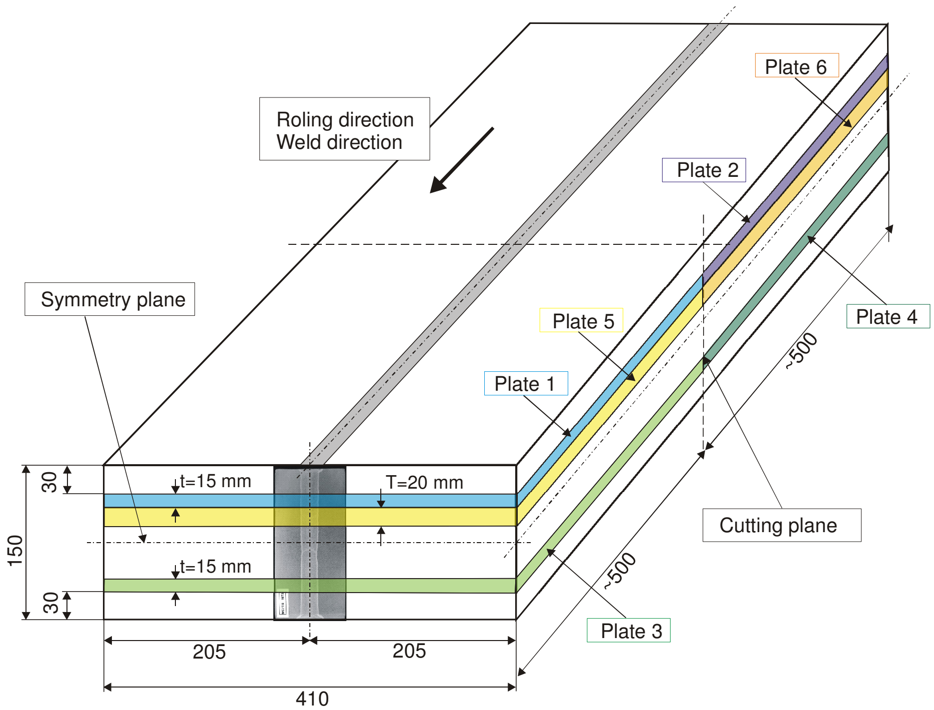

figure 41 Cutting of the thick welded joint into six sub plates for mechanical testing

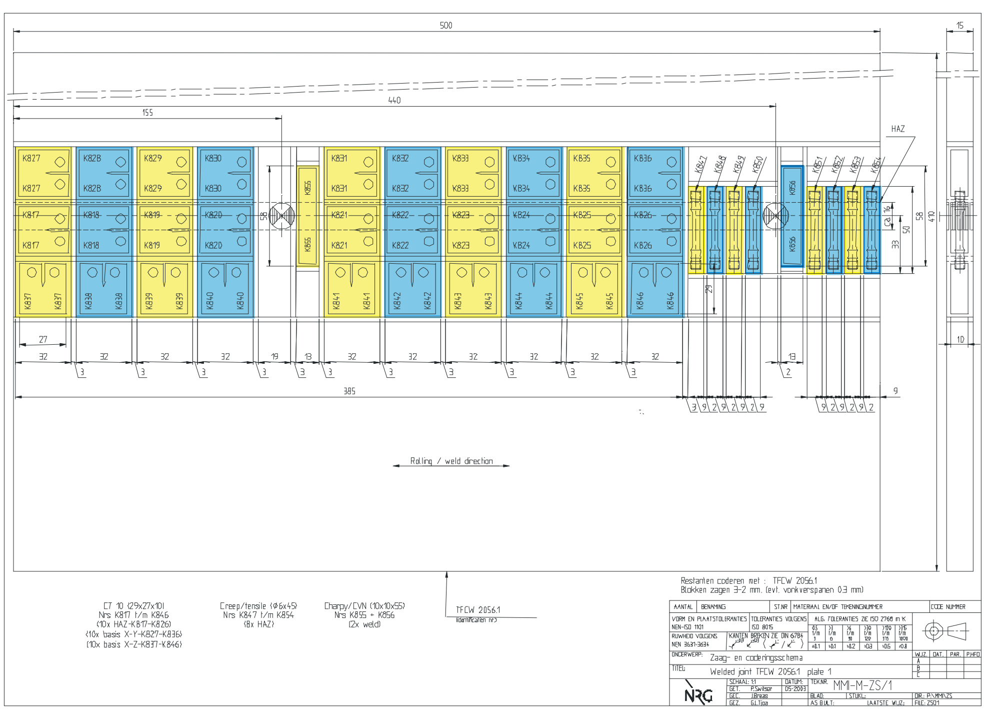

figure 42 Cutting scheme of specimens from TFCW 2056, plate 1

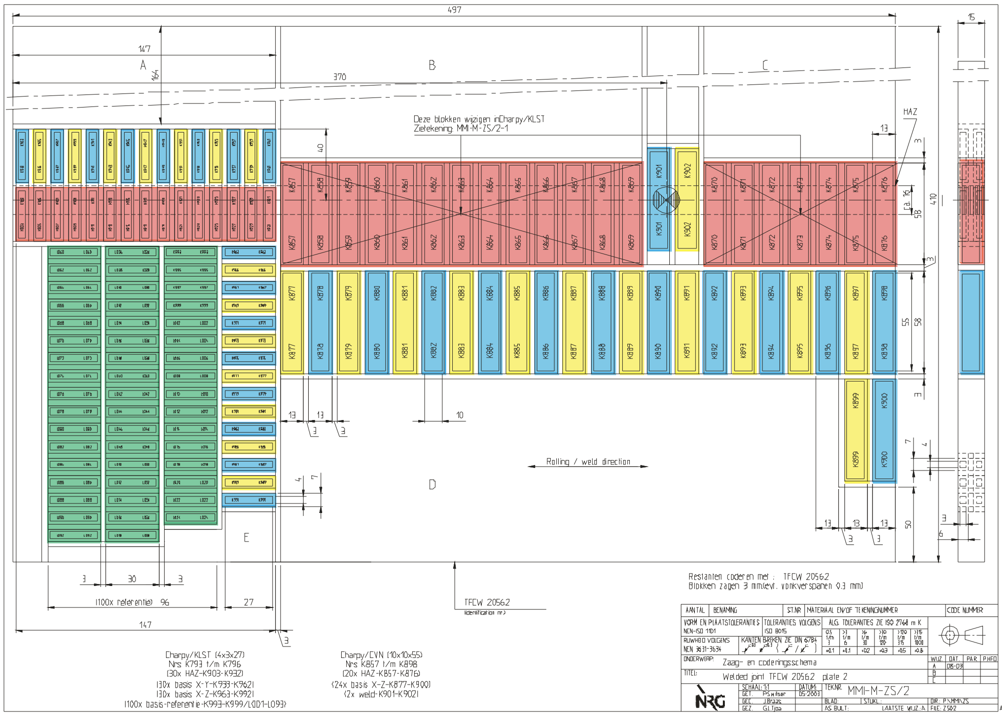

figure 43 Cutting scheme of specimens from TFCW 2056, plate 2

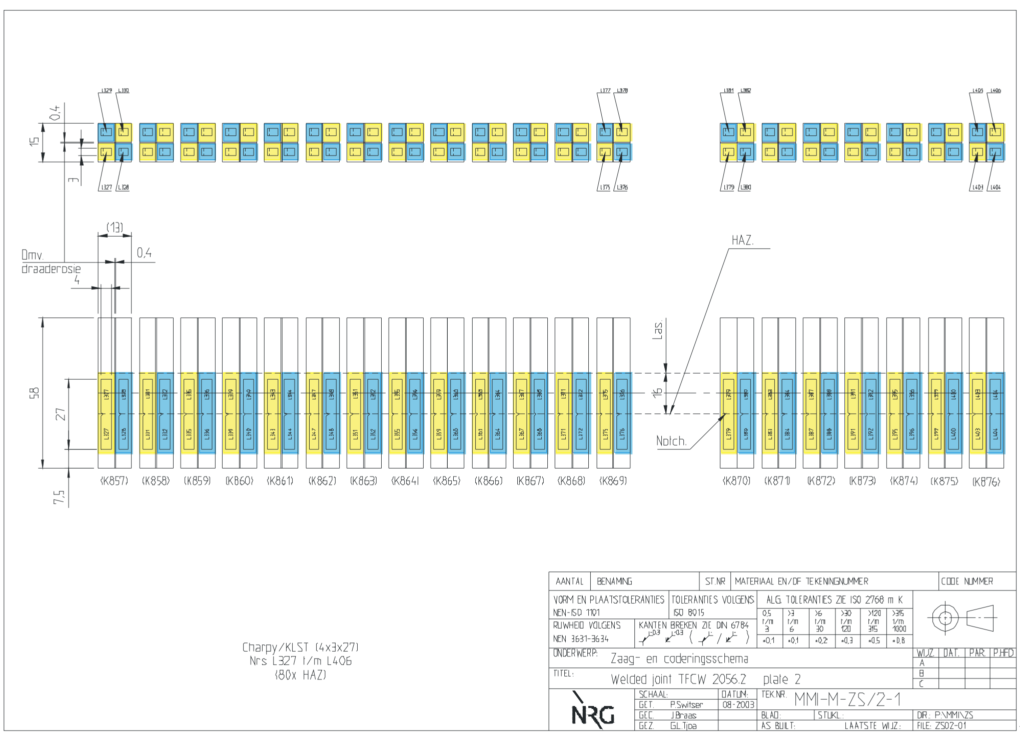

figure 44 Cutting scheme of specimens from TFCW 2056, plate 2a KLST type specimens from full-size Charpy specimens

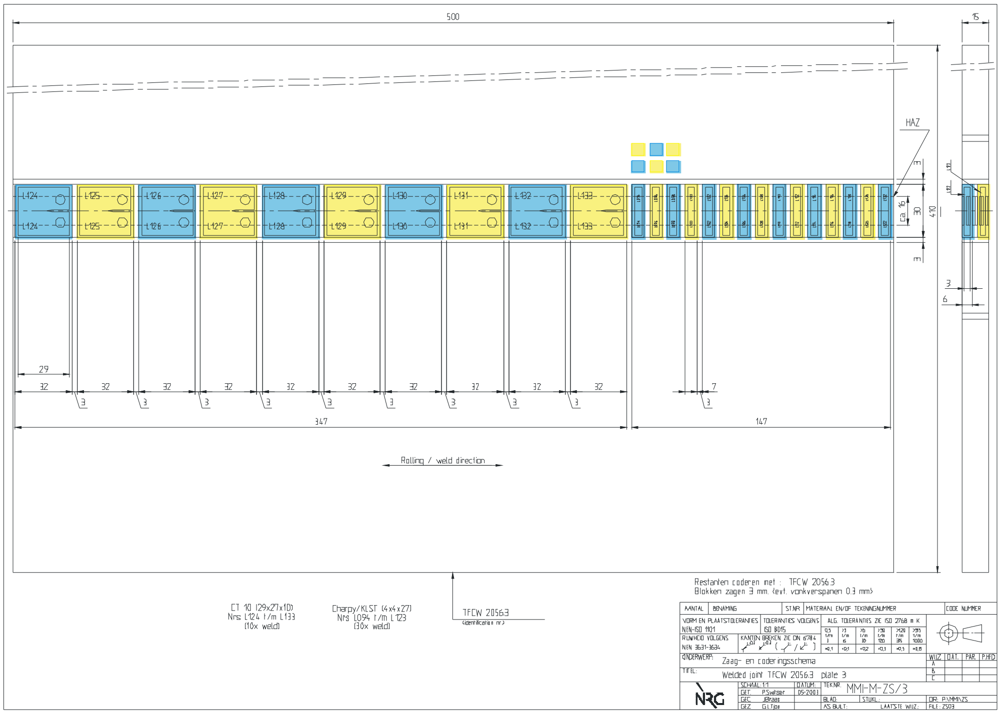

figure 45 Cutting scheme of specimens from TFCW 2056, plate 3

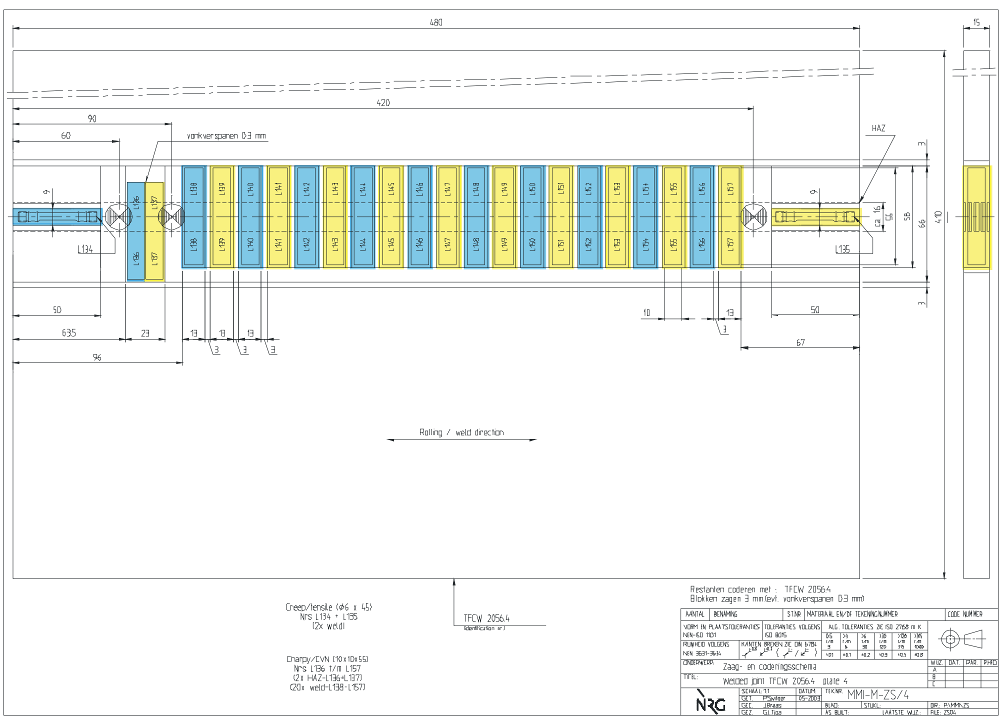

figure 46 Cutting scheme of specimens from TFCW 2056, plate 4

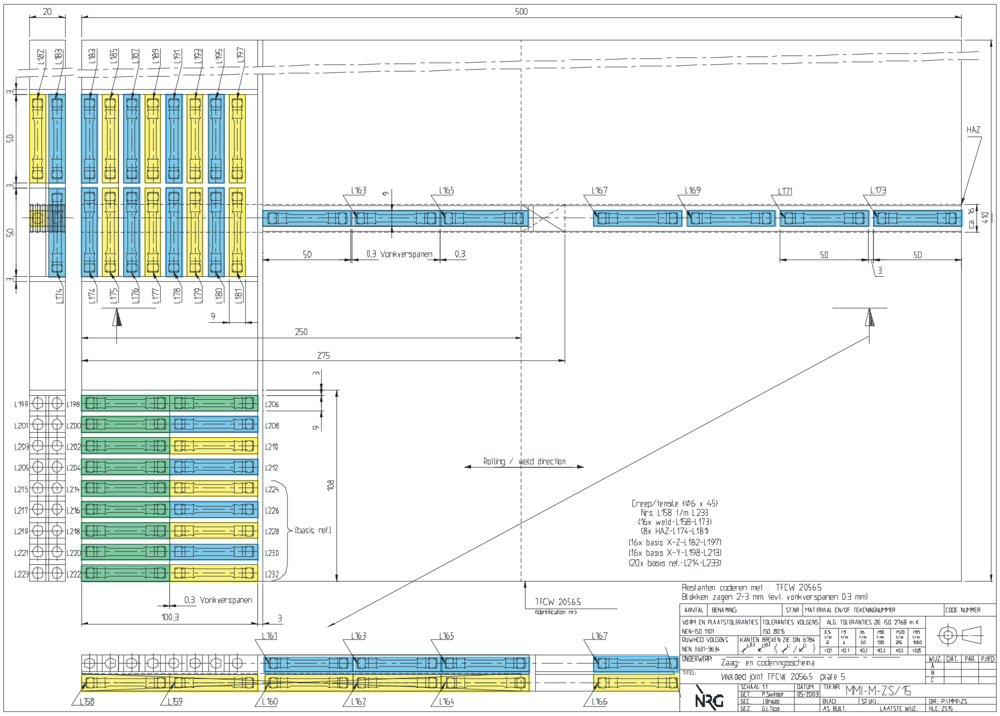

figure 47 Cutting scheme of specimens from TFCW 2056, plate 5

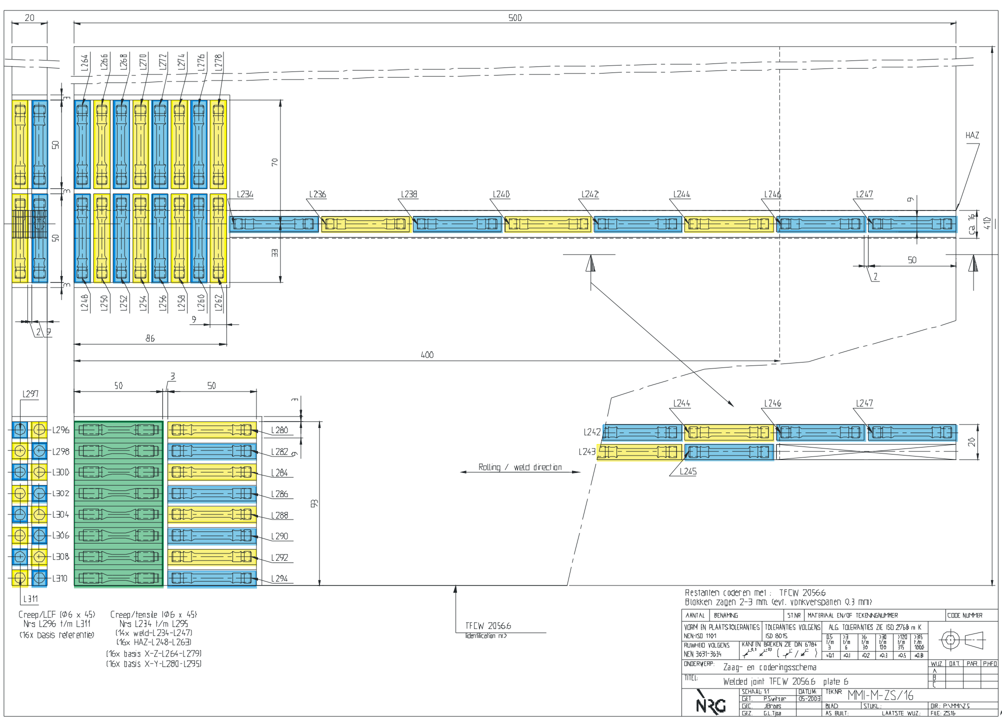

figure 48 Cutting scheme of specimens from TFCW 2056, plate 6

appendix G Loading of the LYRA-08 irradiation capsule

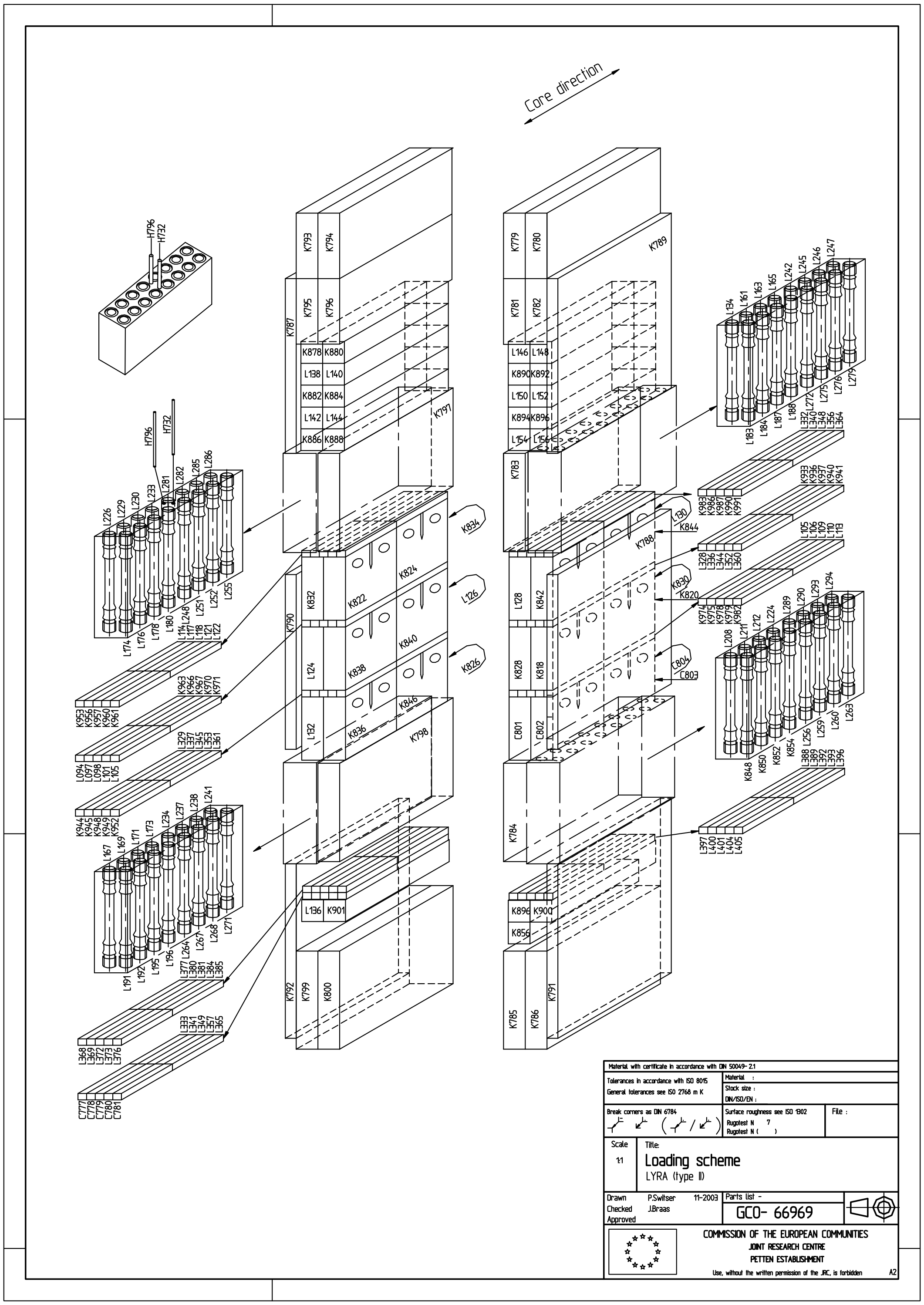

figure 49   Loading configuration of the specimens in LYRA-08